Click here to view linked References

1 **Origin and geodynamic relationships of the Late Miocene to Quaternary alkaline basalt**

2 **volcanism in the Pannonian Basin, eastern-central Europe**

3

4 Szabolcs Harangi[1,2], M. Éva Jankovics[1,3], Tamás Sági[1,2], Balázs Kiss[1,3], Réka Lukács[1,3], Ildikó

5 Soós[1]

6

7 [1] MTA-ELTE Volcanology Research Group, Pázmány sétány 1/C, H-1117 Budapest,

8 Hungary; e-mail: szabolcs.harangi@geology.elte.hu

9 [2] Department of Petrology and Geochemistry, Eötvös University, Pázmány sétány 1/C, H-

10 1117 Budapest, Hungary

11 [3]Vulcano Research Group, Department of Mineralogy, Geochemistry and Petrology,

12 University of Szeged, Egyetem utca 2, H-6722 Szeged, Hungary

13

14 **Abstract**

15 Alkaline basaltic volcanism has been taking place in the Carpathian-Pannonian Region

16 since 11 Ma and the last eruptions occurred only at 100-500 ka. It resulted in scattered low-

17 magma volume volcanic fields located mostly at the margins of the Pannonian basin. Many of

18 the basalts have compositions close to those of the primitve magmas and therefore can be

19 used to constrain the conditions of the magma generation. Low degree (2-3%) melting could

20 occur in the convective asthenosphere within the garnet-spinel transition zone. Melting started

21 at about 100 km depth and continued usually up to the base of the lithosphere. Thus, the final

22 melting pressure could indicate the ambient lithosphere-asthenosphere boundary. The

23 asthenospheric mantle source regions of the basalts were heterogeneous, presumably in small

24 scale, and included either some water or pyroxenite/eclogite lithology in addition to the fertile

25 to slightly depleted peridotite. Based on the prevailing estimated mantle potential temperature

26 (1300-1400°C) along with number of further observations we exclude the existence of mantle

27 plume or plume fingers beneath this region. Instead, we propose that plate tectonic processes

28 controlled the magma generation. The Pannonian basin acted as a thin-spot after the 20-12 Ma

29 syn-rift phase and provided suction in the sublithospheric mantle, generating asthenospheric

30 flow from below the adjoining thick lithospheric domains. A near vertical upwelling along the

31 steep lithosphere-asthenosphere boundary beneath the western and northern margin of the

32 Pannonian basin could result in decompressional melting producing low-volume melts. The

33 youngest basalt volcanic field (Perşani) in the region is inferred to have been formed due to

34 the dragging effect of the descending lithospheric slab beneath the Vrancea zone that could

35 result in narrow rupture at the base of the lithosphere. Continuation of the basaltic volcanism

36 cannot be excluded as inferred from the still fusible condition of the asthenospheric mantle.

37 This is reinforced by the detected low-velocity seismic anomalies in the upper mantle beneath

38 the volcanic fields.

39

42

43 **Introduction**

44   Origin of the basaltic magmas in monogenetic volcanic fields is a key issue to

45 understand the nature of low-magma-flux, episodic, but long lasting volcanic activity (Connor

46 and Conway, 2000; Wang et al., 2002; Aldanmaz et al., 2006; Jung et al., 2006; 2012;

47 Valentine and Perry, 2007; Blondes et al., 2008; Haase and Renno, 2008; Brenna et al., 2012;

48 McGee et al., 2013). Each volcano in such volcanic system is considered to represent eruption

49 of a discrete magma batch ascending rapidly from the mantle source, although recent studies

50 revealed that composition of erupted magmas could change even within the eruptive sequence

of a monogenetic volcano (Strong and Wolff, 2003; Brenna et al., 2010; Erlund et al., 2010; McGee et al., 2012). Apart of these exceptions, basalts of monogenetic volcanoes provide a unique snapshot of the nature of the mantle source regions and could reveal their subtle compositional differences. Furthermore, basaltic products having composition close to the primitive magmas can be used to infer the condition of the mantle generation (pressure and temperature, mineral and chemical composition of the melted mantle rock, degree of melting, mixing of melts etc.). Using this knowledge, a better understanding can be achieved about the triggering mechanism of the melt generation and the geodynamic relationships of the volcanism. Nevertheless, recent studies have revealed that evolution of basaltic magmas could be far more complex than previously thought (Woodland and Jugo, 2007; Smith et al., 2008; Jankovics et al., 2012; 2013) and careful investigation is necessary to select the most appropriate samples, which can be used to gain insight into the mantle and the melting process.

The Carpathian-Pannonian region (CPR; Fig. 1.) is a key natural laboratory for studying the interaction of deep mantle processes, igneous activity and tectonic events (Szabó et al., 1992; Seghedi et al., 1998; 2004a; 2004b; 2005; Harangi, 2001a; Konečný et al., 2002; Harangi and Lenkey, 2007; Seghedi and Downes, 2011). Alkaline basalt monogenetic volcanic fields have developed since 11 Ma, partly overlapping and partly postdating the extensive calc-alkaline andesitic-dacitic volcanism (Pécskay et al., 2006; Lexa et al., 2010). The alkaline basaltic volcanism is considered as part of the widespread Neogene to Quaternary volcanism in western and central Europe (Wilson and Downes, 1991; 2006; Embey-Isztin and Dobosi, 1995; Lustrino and Wilson, 2007), but it shows many similarities also with the alkaline basaltic volcanism occurred with close spatial and temporal association of calc-alkaline and potassic-ultrapotassic volcanism in the Mediterranean (Wilson and Bianchini, 1999; Harangi et al., 2006; Beccaluva et al., 2011). The origin of the basaltic

76 volcanism in the CPR is still controversial (Embey-Isztin and Dobosi, 1995; Embey-Isztin et

77 al., 2001; Harangi, 2001a; 2001b; Seghedi et al., 2004a; Harangi and Lenkey, 2007; Ali and

78 Ntaflos, 2011; Ali et al., 2013; Harangi et al., 2013), largely due to its occurrence after the

79 main extensional phase of the Pannonian basin. Eruption of basaltic magmas took place even

80 at a couple of 100's ka, thus, understanding the mechanism of melt generation is crucial also

81 to evaluate rigorously whether this kind of volcanic activity could continue in the future.

82   In this paper, we discuss the conditions of the basaltic magma generation in the CPR

83 using primarily those samples, which have chemical composition close to primitive magmas.

84 We combine major and trace element data of the host basalts as well as compositional features

85 of spinels, one of the liquidus minerals in these rocks, to constrain the origin of the magmas

86 and the nature of the source regions. Then, we propose a possible mechanism that could be

87 responsible for the formations of the basaltic volcanoes in this region.

88

89 **Geological setting**

90

91   The Carpathian-Pannonian region lies in the northeastern part of the Alpine-

92 Mediterranean region and is characterized by an arcuate orogenic belt (Carpathians) with a

93 basin area behind it (the Pannonian basin; Fig. 1A). The Pannonian basin is surrounded by the

94 Alpine, Carpathian and Dinarides mountain belts. It is underlain by thin lithosphere (50-80

95 km) and crust (22-30 km) coupled with high heat flow (>80 mW/m^2; Csontos et al., 1992;

96 Horváth, 1993; Tari et al., 1999; Lenkey et al., 2002; Horváth et al., 2006). It is regarded as a

97 special type of back-arc basin formed by heterogeneous stretching of the lithosphere. The

98 thinning of the lithosphere started in the Early Miocene (around 20 Ma) and the syn-rift phase

99 was finished by the end of Miocene (around 12 Ma; Horváth et al., 2006). Tari et al. (1999)

100 defined an initial core-complex style extension during the Early Miocene followed by a wide-

101 rift type extension. Huismans et al. (2001) distinguished two main rifting events, involving a

102 Middle Miocene passive rifting followed by a Late Miocene active rifting episode. As a

103 consequence, the lithospheric mantle underwent a dramatic attenuation (stretching factor of

104 5–50), whereas the crust was only moderately thinned (stretching factor of 1.2–2.5) leading to

105 the suggestion of an inhomogeneous stretching model (Sclater et al., 1980; Horváth et al.,

106 1988; 2006). As an extreme case, Horváth et al. (2006) assumed the disappearance of the

107 whole mantle lithosphere beneath the Pannonian Basin at the beginning of the synrift phase.

108 The thinning of the lithosphere was accompanied by asthenospheric mantle updoming as

109 shallow as 50-60 km (Stegena et al., 1975; Huismans et al., 2001; Konečný et al., 2002) and

110 therefore, the Pannonian basin can be considered as one of the hottest basin areas of Europe

111 (Cloetingh et al., 2007). The syn-rift phase was followed by post-rift thermal subsidence,

112 when several thousands meters of Late Miocene to Quaternary sediments filled parts of the

113 basin areas (Great Hungarian Plain, Little Hungarian Plain).

114 There are diverse views on the driving mechanism of the lithospheric extension such

115 as (a) formation of an overthickened hot lithosphere, which underwent gravitational collapse

116 during the Early Miocene (Tari et al., 1999; Horváth et al., 2006); (b) suction of the slab roll-

117 back beneath the retreating subduction along the Eastern Carpathians (Csontos et al., 1992);

118 (c) dripping the lower, gravitationally instable lithospheric material into the deep mantle

119 (Lorinczi and Houseman, 2000) and (d) asthenospheric flow either via the "Istria window"

120 beneath the Dinarides (Horváth and Faccenna, 2011) or from the Adria–European collision

121 zone and ensuing Alpine orogeny (Kovács et al., 2012). While the models (a) and (b) are

122 supported by geophysical and geological observations and are widely accepted by the

123 scientific community, the novel models (c) and (d) have still a number of inconsistencies and

124 therefore need more supporting evidences.

125   Since the Pliocene, the CPR has been in a tectonic inversion stage (Horváth and

126   Cloetingh, 1996; Bada et al., 1999) due to the continuous push from west (Adria-push from

127   the Alps–Dinarides belt) and blocking the area at east by the thick Ukrainian lithosphere. The

128   entire basin system has been landlocked and this led to a gradual structural inversion in the

129   form of multi-scale folding and fault reactivation. Some parts of the CPR (Great Hungarian

130   Plain, Little Hungarian Plain and Danube basin, Vienna basin, Styrian basin and Brasov

131   basin) are still subsiding, while other parts show uplift (Dombrádi et al., 2010). This

132   differential vertical movement is accommodated by reactivation of older faults. Major strike-

133   slip faults have a SW-NE orientation at the northern and central part of the CPR, whereas to

134   the south a characteristic E-W trending strike-slip fault system was identified (Horváth et al.,

135   2006; Fig. 1B).

136   The nature of the upper mantle beneath the CPR is inferred from seismic tomographic

137   models. These show a high-velocity body in the transition zone (400-670 km) interpreted as

138   accumulated subducted slab material (Wortel and Spakman, 2000; Piromallo and Morelli,

139   2003; Hetényi et al., 2009), a near-vertical high-velocity slab beneath the southeastern margin

140   of the CPR (Vrancea zone), regarded as the trace of final-stage subduction (Sperner et al.,

141   2001; 2004) and relatively low velocity material between the transition zone and the base of

142   lithosphere.

143

144   **Areal distribution of the basalts**

145

146   In the CPR, four main monogenetic volcanic fields were developed (Styrian, Bakony-

147   Balaton Upland, Nógrád-Gemer, Perşani; Fig. 1B). In addition, localized basaltic centres were

148   developed in a few areas (Pauliberg-Oberpullendorf in Burgenland, Lucaret-Sanovita in

149   Banat), where no precursor and subsequent volcanism occurred. Basalt volcanic centres of the

150   eastern part of the Little Hungarian Plain (called here Kemenes Volcanic Field, Fig. 1B) and

151   around Štiavnica (ST in Fig. 1B) can be considered to form ultra-low-magma-flux volcanic

152   fields, where volcanic activity was sporadic (<10 volcanic centres) during a considerable (2-6

153   Myr) timescale and characterized by several 100's ka (several Myr in ST) long quiescence

154   time between the active events.

155   The basaltic volcanism was controlled by external conditions, such as tectonics,

156   topography, presence and style of aquifer in the basement (Martin and Németh, 2004;

157   Kereszturi et al., 2011). Tuff rings and maar structures were developed as a result of

158   phreatomagmatic explosive eruptions followed occasionally by pure magmatic explosive

159   volcanism and in a few cases lava lakes were formed in the late-stage effusive phase. Large

160   volcanic edifices, such as shield volcanoes were built up in each volcanic field (Stradner

161   Kogel in Styria, Kab, Agár and Fekete hills in the Bakony-Balaton Upland, Medvedia in

162   Nógrád-Gemer) except for the Perşani. The volcanism was dominantly basaltic, the only

163   exception is the Kemenes Volcanic Field, where a large trachyandesite-trachyte volcano

164   developed around 10-11 Ma (Pásztori volcano; Harangi et al., 1995; Harangi, 2001b). This

165   volcano subsided subsequently and was covered by thick (over 2000 m) Late Miocene to

166   Quaternary sediments.

167   The geographic location of the volcanic fields in the CPR (Fig. 1B) is remarkable,

168   since they are mostly at the western and northern margins of the Pannonian basin and not in

169   the central area, where there is the thinnest lithosphere, whereas the youngest one is found at

170   the southeastern part of the region, close to the seismically active Vrancea zone. The two

171   largest volcanic fields in the CPR are the Bakony-Balaton Upland Volcanic Field (Martin and

172   Németh, 2004) and the Nógrád-Gemer Volcanic Field (Konečný et al., 1995; 1999), each of

173   them involves about 50 eruptive centres, have relatively long timescale of the volcanism (6-8

174   Ma) and includes intermittent active phases with relatively long (several 100's ka) repose

175   time. Kereszturi et al. (2011; 2013) calculated the recurrence rate for both volcanic fields and

176   got about 0.11 and 0.08 Ma/event, respectively. Although the volcanic edifices are deeply

177   eroded in both areas, they estimated also the magma-flux that is 0.9 km^3/Ma (calculated only

178   for the last 5 active phases, excluding the initial phase) and 0.4 km^3/Ma, respectively (the total

179   erupted magma volume is estimated to be about 4 and 3.5 km^3, respectively). These numbers

180   are comparable with the low magma-flux monogenetic volcanic fields, such as the

181   Southwestern Nevada Volcanic Field (Valentine and Perry, 2007) and classify them as typical

182   tectonically-controlled, time predictive volcanic fields. The Styrian and Perşani Volcanic

183   Fields (Seghedi and Szakács, 1994; Downes et al., 1995; Ali and Ntaflos, 2013; Harangi et al.,

184   2013) contain less eruptive centres, although in Styria, the eruptive volume could be relatively

185   large (>1 km^3 total volume) due to the significant amount of effusive volcanic products

186   (Stradner Kogel, Klöch, Steinberg). The Perşani Volcanic Field is the youngest one in the

187   CPR and is located in a 22 km long and 8 km wide area (Seghedi and Szakács, 1994) at the

188   northwestern periphery of the intramontane Braşov basin (Fig. 1B.). This area is characterized

189   by NE-SW trending normal faults, resulting from a NW-SE extensional regime (Gîrbacea et

190   al., 1998). The eruptive centres appear to be structurally controlled and show a rough NE-SW

191   trending alignment. Popa et al. (2012) recorded subcrustal seismicity beneath the Perşani area

192   and, using seismic tomography modelling, suggested that a low-velocity anomaly could be

193   inferred at the crust-mantle boundary. The youngest basalt volcano (Putikov vŕšok; Šimon and

194   Halouzka, 1996) of the CPR is located near Banska Štiavnica upon the Late Pleistocene

195   terrace of the river Hron. It does not rigorously belong to the Nógrád-Gemer Volcanic Field

196   and was formed after more than 6 Ma quiescence in this area. There are two 'satellite

197   volcanoes" in the CPR: The alkaline basalts of Pauliberg and Oberpullendorf are found at the

198   Alps-Pannonian Basin transition zone in Burgenland (Harangi, 2001b; Ali and Ntaflos, 2011)

199   and represent a single volcanic episode at about 11 Ma. Harangi et al. (1995) suggested that

200   they could have some compositional similarities with the basaltic dyke rocks in the Pásztori

201   volcano. In the southern part of the CPR, the alkaline basalt of the Lucaret-Sanovita belongs

202   also to a single eruptive event without any precursor magmatism. It is located close to a major

203   west-east trending strike-slip zone (Fig. 1B) and at the boundary of subsiding and uplifting

204   areas (Dombrádi et al., 2010). Remarkably, further single – potassic-ultrapotassic - volcanoes

205   (Bár, Uroi) were formed also along this tectonic line during the last 2.5 Ma.

206

207   **Temporal evolution**

208

209   Monogenetic basalt volcanic fields are typically active over millions of years. The

210   volcanism is characterized by intermittent eruptions gathering often in active phases, which

211   are separated by long repose periods. Recurrence rate of volcanism is particularly important in

212   evaluating the volcanic hazard (Condit and Connor, 1996; Valentine and Perry, 2007),

213   although precise dating of eruptions is difficult for basaltic rocks. In the Pannonian Basin,

214   eruption ages were determined mostly by K/Ar radiometric technique (Balogh et al., 1982;

215   1986; 1990; 1994; Borsy et al., 1986). Ar/Ar dating was performed for the basaltic rocks of

216   the Bakony-Balaton Upland volcanic fields that corroborated the reliability of the former

217   K/Ar data (Wijbrans et al., 2007). In contrast, the new Ar/Ar age data (Panaiotu et al., 2013)

218   refined significantly the former knowledge (Panaiotu et al., 2004) on the temporal evolution

219   of the Perşani volcanic field. So far, the available K/Ar data base provides a solid framework

220   for the temporal evolution of the alkaline basaltic volcanism in the Pannonian basin, although

221   more careful studies are necessary to define the recurrence rates in individual volcanic fields

222   more precisely and constrain the eruption age of the youngest volcanic episodes.

223   In the Pannonian Basin, eruption of alkali basaltic magmas started in the westernmost

224   margin, where two outcrops are known, at Pauliberg and at Oberpullendorf in Burgenland

225   (Ali and Ntaflos 2011) and their ages were determined as 11.7 to 10.5 Ma (Balogh et al.,

226   1994). Similar ages were published for the basalts found in drilling cores around Kecel

227   (central Pannonian basin; 8.1-10.4 Ma; Balázs and Nusszer 1987). Although these basalts are

228   strongly altered, their Late Miocene ages were corroborated by stratigraphic data.

229   The basaltic volcanism in the two largest volcanic fields (Bakony-Balaton Upland and

230   Nógrád-Gemer) lasted for more than 6 Myr. Noteworthy, eruption of basaltic magmas in both

231   areas commenced at 7.8-8.0 Ma (Balogh and Németh, 2005; Balogh et al., 2005; Chernyshev

232   et al., 2013) and continued after 2 Ma quiescence in the Bakony-Balaton Upland and after

233   about 1 Ma repose time in the Nógrád-Gemer area. The volcanism in both areas was

234   characterized by closely packed active phases separated by long repose periods (Konečný et

235   al., 1995; 1999; Wijbrans et al., 2007). Kereszturi et al. (2013) estimated the peak magma

236   output times being at 3-4 Ma in the Bakony-Balaton Upland volcanic field and 1.5-3.0 Ma in

237   the Nógrád-Gemer area. The alkaline basalt occurrences cropping out within the area of the

238   Middle Miocene eroded andesitic Štiavnica composite volcanic complex are spatially

239   separated from the Nógrád-Gemer volcanic field. They show highly sporadic eruption times,

240   such as 6.6-7.8 Ma in Banska Štiavnica and Dobrá Niva and 0.1-0.5 Ma for the Putikov

241   volcano at the Hron river (Balogh et al., 1981; Konečný et al., 1999; Šimon and Halouzka,

242   1996; Šimon and Maglay, 2005; Chernyshev et al., 2013). The age of the Putikov vŕšok

243   volcano has a particular importance, since it indicates the latest alkaline basalt eruption in the

244   CPR. Balogh et al. (1981) and later, Chernyshev et al. (2013) provided 430-530 ka eruption

245   ages using K/Ar technique, whereas Šimon and Halouzka (1996) considered the stratigraphic

246   position of the lava flow and interpreted it as sitting on the Late Pleistocene (Riss) terrace of

247   the Hron river and this points to an age of 120-150 ka. This younger age was supported by

248   optically stimulated luminescence (OSL) dating of the underlying sediments that yielded an

249   age of 102± 11 ka. Further investigation is necessary and highly important to constrain the

250   exact eruption age of this basalt. The youngest eruption ages in the Nógrád-Gemer volcanic

251   field require also detailed investigation. In the last intense eruptive phase between 1.1-1.5 Ma,

252   mostly effusive activity was recognized (Konečný et al. 1995; 1999). The latest eruptions in

253   this area was previously thought to have occurred around 400 ka (Hodejov and Fil'akovo

254   maars; Konečný et al. 1995), however, new (U-Th)/He zircon dating (Hurai et al., 2013) did

255   not confirm this young age.

256   In the western margin of the CPR (Styrian basin; Ali et al., 2013), alkaline basaltic

257   volcanism occurred between 3.9 and 1.9 Ma (Balogh et al., 1994) after a long quiescence

258   period since the 14.0-17.5 Ma high-K trachyandesitic volcanic activity (Harangi et al., 1995).

259   The latest eruption resulted in a relatively large volume shield volcano composed of

260   nephelinites at Stradner Kogel.

261   The youngest monogenetic volcanic field of the CPR is located at the western margin

262   of the Perşani Mts., between the Transylvanian basin and the Brasov basin (Seghedi and

263   Szakács, 1994; Downes et al., 1995; Harangi et al., 2013). Although former K/Ar and

264   palaeomagnetic dating (Panaiotu et al., 2004) implied two, well separated eruption phases, the

265   new Ar/Ar dating (Panaiotu et al., 2013) revised this and indicated a fairly continuous, but

266   very scattered volcanism from 1.22 Ma to 0.52 Ma.

267   Finally, a unique basalt occurrence is found at Lucaret (southern Pannonian basin),

268   where no precursor volcanic activity took place and the age of this basalt was determined as

269   2.4 Ma (Downes et al., 1995).

270

271   **Petrologic and geochemical characteristics**

272

273   Petrologic and geochemical features of the alkaline basaltic rocks of the CPR have

274   been published in several papers (Embey-Isztin et al., 1993; 2001; Seghedi and Szakács,

11

275   1994; Dobosi et al., 1995; Downes et al., 1995; Harangi et al., 1995; 2013; Harangi, 2001b;

276   Harangi and Lenkey, 2007; Ali and Ntaflos, 2011; Tschegg et al., 2010; Jankovics et al.,

277   2012; 2013; Ali et al., 2013) and we completed them with new analysis, mostly from the

278   Nógrád-Gemer Volcanic Field (Sági et al., 2013). Representative composition of the basalts

279   from different locations is given in Table 1. In this section, we provide a brief summary on the

280   main features of the basalts.

281   The basaltic rocks are classified as alkali basalts, trachybasalts, basanite,

282   phonotephrite and nephelinite (Fig. 2). Evolved rocks types occur in the buried Pásztori

283   volcano, they are trachyandesite and trachyte (Harangi et al., 1995; Harangi, 2001b). Most of

284   the basalts are olivine-phyric, while clinopyroxene phenocryst is found in a few localities of

285   the Bakony-Balaton Upland and Kemenes Volcanic Field, but is more common in the basalts

286   of the Styrian Volcanic Field and in the Nógrád-Gemer Volcanic Field. The olivine

287   phenocrysts with Fo>84 mol% often contain spinel inclusions and these two minerals can be

288   regarded as liquidus phases. Both minerals have a wide compositional range (Embey-Isztin et

289   al., 2007; Ali and Ntaflos, 2011; Jankovics et al., 2012; 2013; Ali et al., 2013; Harangi et al.,

290   2013). The most magnesian olivines have typically high Mn content compared with the trend

291   defined by Herzberg (2011) for olivines crystallized from peridotite-derived magmas. They

292   are characterized by low Fe/Mn ratio (Fe/Mn=40-75); this feature along with the relatively

293   low Ni content (<2500 ppm) is not consistent with derivation of the primary magmas from

294   pyroxenite source as defined by Sobolev et al. (2007) and Herzberg (2011). Clinopyroxene

295   phenocrysts could have crystallized mostly at the crust mantle boundary zone as shown by the

296   geobarometric calculations. Their complex zoning often found in basalts from the Nógrád-

297   Gemer and the Bakony-Balaton Upland indicates mixing of magma batches at depth (Dobosi,

298   1989; Dobosi and Fodor, 1992). Mantle-derived ultramafic and lower crustal granulite

12

299 xenoliths are common in basalts of each volcanic field (Embey-Isztin et al., 2001; Szabó et

300 al., 2004).

301   The CPR basalts are almost exclusively silica-undersaturated and have mg-numbers

302 ranging from 0.5 to 0.8 (MgO=5-15 wt%). The most magnesian basalts contain, however,

303 significant amount of xenocrysts (e.g., Bondoró and Füzes at Bakony-Balaton Upland), which

304 strongly modify the bulk rock composition (Jankovics et al., 2012; 2013). Majority of the

305 basalts have an mg-number >0.62 suggesting only a minor to moderate effect of fractional

306 crystallization. Moderately fractionated basalts are found mostly in Styria and in the Nógrád-

307 Gemer areas. For this study, we selected those samples that have mg-number between 0.64

308 and 0.72 (MgO=8-13 wt%) and therefore their compositions are close to that of the primitive

309 magmas. In these samples, variation of major elements indicates the controlling factor of

310 various amounts of olivine fractionation. However, characteristic differences can be

311 recognized between the most primitive basalts. The Pauliberg basanite has a distinct

312 composition with low Al_2O_3 and high TiO_2 and FeO contents (Fig. 3). Experimental studies

313 suggest that such composition could be obtained by low-degree melting of carbonated, silica-

314 deficient eclogite (Dasgupta et al., 2006; Kogiso and Hirschmann, 2006). The basalts from

315 Oberpullendorf (Burgenland) and Putikov vŕšok (Štiavnica) have a transitional major element

316 composition between the Pauliberg basanite and the rest of the CPR basalts.

317   The trace element composition of basalts resembles those commonly found in intra-

318 plate magmas and is similar to the Neogene to Quaternary alkaline mafic rocks in Western

319 and Central Europe (Wilson and Downes, 1991; Lustrino and Wilson, 2007). The FTS

320 elements, such as Ni, Cr and Sc have relatively high abundances (Ni=100-300 ppm; Cr=100-

321 500 ppm; Sc=10-30 ppm; Fig. 3) consistent with the slight olivine±spinel-dominated

322 fractional crystallization. Based on the primitive mantle (McDonough and Sun, 1995)

323 normalized trace element patterns, Harangi and Lenkey (2007) defined two main

324   compositional groups: the first one is characterized by stronger enrichment in incompatible

325   trace elements and a typical negative potassium anomaly, whereas the second one has

326   smoother trace element patterns and no negative potassium anomaly (Fig. 4). The strongly

327   incompatible trace elements have a wide compositional range (La=25-90 ppm, Nb=30-130

328   ppm, Th=3-13 ppm; Fig. 3) and show a positive correlation with an intercept of zero. Same

329   covariance with Ba can be also observed although the basalts from Pauliberg and Styria show

330   a distinct trend.

331   Sr-Nd-Pb isotope ratios of the basalts were published by Embey-Isztin et al. (1993),

332   Dobosi et al. (1995), Downes et al. (1995) and Harangi et al. (1995). All of the basalts fall

333   into the depleted field in Sr-Nd isotope space, similarly to majority of the Neogene to

334   Quaternary alkaline mafic rocks in Western and Central Europe (Wilson and Downes, 1991;

335   Wilson and Patterson, 2001). The most depleted end-member of this variation trend is a

336   mixture of HIMU and DMM. In the Pb-Pb isotopic diagrams, they show a relatively large

337   variation, many of the samples have relatively high $^{207}Pb/^{204}Pb$ ratio (>15.6) causing a vertical

338   shift from the NHRL. The highest $^{206}Pb/^{204}Pb$ ratio (19.6-19.7) is shown by the Pauliberg

339   basanite.

340

341   **Discussion**

342

343   Most of the alkaline basalts of the CPR show chemical composition (MgO>8 wt%;

344   Ni=130-350 ppm; Fig. 3) that could be close to that of the primitive magmas. Using only

345   these samples, the condition of the melting process as well as the nature of the source region

346   can be constrained that could contribute to our understanding on the reason of mantle melting

347   beneath the area. Trace element ratios such as Nb/Th (5–15) and Nb/La (1–2) of the basalts

348   show values that are higher than those observed in continental crustal rocks (Rudnick and

14

Fountain, 1995) and are typical of mantle-derived melts, mostly for those derived from the

asthenosphere. Therefore, we can conclude that crustal contamination did not significantly

modify the trace element composition of the CPR mafic magmas. Most of the selected basalts

are olivine-phyric and the olivine phenocrysts often contain spinel inclusions indicating that

these mineral phases could have been liquidus minerals as have been suggested for the usual

evolution of alkaline silica-undersaturated mafic magmas (Roeder et al., 2006). High pressure

clinopyroxene crystallization could modify the magma composition as well as the

composition of coexisting evolving phases and this should be considered even in the absence

of clinopyroxene phenocrysts in the rocks (Smith et al., 2008). This would decrease the CaO

content of the magma and possibly also leads to lowering the CaO content of the olivine

phenocrysts. Nevertheless, our geothermobarometric calculations on selected clinopyroxenes

in some basalts (Harangi et al., 2013) suggest that they crystallized later then the olivines. The

relatively high Sc content of the basalts (Sc>15 ppm except for the samples from Lucaret) and

the uniform Cr-number of the spinels along with various Fo content of coexisting olivines

also imply that no significant early-stage clinopyroxene fractionation occurred that would

significantly modify the magma composition. Taking all of this into account, the composition

of the alkaline basalts with MgO>8 wt% can be used to infer the melting condition and the

nature of the source rock.

In this discussion, we attempt to constrain the origin of the magmas using the

following principle: we consider the simplest model over the complex models and take a

complex model only when no simple model works (Niu, 2005). Thus, we simplified the

mantle source material considering to be dominantly peridotitic in lithology, knowing,

however, that involvement of more fusible material, such as pyroxenite or eclogite could be

possible. There are some inferences for the existence of such material in the mantle source

373   region, but we think that further, careful investigation is necessary to test their influence on

374   the melting models and the composition of the primary magmas.

375

376   *Asthenospheric vs. lithospheric mantle source region*

377

378   Origin of the continental intraplate basaltic rocks is often debated. Alkaline silica-

379   undersaturated mafic magmas are considered being generated by low-degree of melting either

380   in the upwelling asthenosphere (Bradshaw et al., 1993; Wang et al., 2002; Niu et al., 2011;

381   Gazel et al., 2012) or by melting of metasomatic, usually amphibole-rich veins in the

382   lithosphere (Fitton et al., 1991; Ormerod et al., 1991; DePaolo and Daley, 2000; Beccaluva et

383   al., 2007; Valentine and Perry, 2007; Bianchini et al., 2008; Pilet et al., 2008; Mayer et al.,

384   2013; 2014). Variation of trace element and isotopic compositions of the Neogene to

385   Quaternary basaltic rocks in Europe led Wilson and Downes (1991; 2006) to conclude that

386   both mantle regions could have contributed to the magma generation. This was reinforced by

387   the more specific studies in various parts of volcanic areas in Europe (Haase et al., 2004;

388   Haase and Renno, 2008; Jung et al., 2012), including the Pannonian basin (Embey-Isztin and

389   Dobosi, 1995; Harangi, 2001a; Seghedi et al., 2004) and was suggested also for the origin of

390   the basaltic magmas in the western USA (Fitton et al., 1988; 1991), in the Auckland volcanic

391   field, New Zealand (McGee et al., 2013) and western Syria (Ma et al., 2011). However, an

392   important question is why the colder lithospheric mantle undergoes melting. For this, the

393   presence of fusible material (metasomatic veins) and either significant thinning of the

394   lithosphere or a thermal perturbation (heating) are necessary. The fusible material is usually

395   considered to be amphibole-bearing veins, which originated from low-volume asthenospheric

396   melts and are frozen in the lower lithosphere (McKenzie, 1989; Niu, 2008; Pilet et al. 2008;

397   Humphreys and Niu, 2009). The presence of amphibole in the source region is usually

16

398   inferred based on the negative K-anomaly in the primitive mantle normalized trace element

399   patterns (Class and Goldstein, 1997; Späth et al., 2001; Jung et al., 2005; Haase and Renno,

400   2008). Amphibole is stable up to about $1100^{o}C$ temperature and up to about 2.5-3.0 GPa (ca.

401   100 km depth) and is regarded to be confined to the lithospheric mantle (Wallace and Green,

402   1991).

403   The negative K-anomaly as expressed by the K/K* ratio (calculated as

404    $K_N/\sqrt{(Nb_N*La_N)}$, where K_N, Nb_N and La_N are primitive mantle normalized values) is a

405   characteristic feature of many of the CPR basalts and shows a wide continuous range

406   (K/K*=0.3-1.2; Fig. 5). It has a negative correlation with the La/Y and $(Sm/Yb)_N$ ratios,

407   which are the indicators of the degree and the relative depth of melting. This could suggest

408   that a K-bearing phase, presumably amphibole was present in the source of all of the CPR

409   magmas and remained in the residual mantle during low degree melting and entered into the

410   melt in the case of larger melting. In that situation, the source of the magmas should be

411   entirely the lithospheric mantle. Melting of the lower lithosphere in the post-rift phase of the

412   Pannonian basin cannot be explained by decompression-driven process, but only by thermal

413   perturbation, i.e. via heat flux from the underlying asthenospheric mantle. Taking this view,

414   Seghedi et al. (2004b) postulated localized mantle plumes (plume fingers) beneath the basalt

415   volcanic fields of the CPR. However, there is lack of physical evidences for the generation of

416   localized hot mantle upwelling scattered beneath the Carpathian-Pannonian region and there

417   is a lack of explanation why this does not occur beneath the central Pannonian basin, where

418   there is the thinnest lithosphere. Furthermore, the lowest K/K* value is shown by the basalts

419   having the highest $(Sm/Yb)_N$ ratios and therefore reflect garnet in the source region. This

420   would mean melting at depth greater than 80 km, which is already the asthenospheric mantle

421   beneath most part of the region. Nevertheless, theoretically, it is possible that the high

422    $(Sm/Yb)_N$ ratio is inherited in the metasomatic vein (Pilet et al., 2008). Although Pilet et al.

17

423 (2008) claimed that preferential melting of this material would yield magma composition akin

424 to alkaline mafic magmas, others suggest that in this case potassic magmas are generated

425 (McKenzie, 1989; Wilson and Downes, 1991; Cebriá and López-Ruiz, 1995). Furthermore,

426 the K/K* ratio in the CPR basalts has no correlation with the La/Nb ratio that is used as an

427 indicator of the lithospheric mantle (Fitton et al., 1991). In addition, the La/Nb ratio of the

428 CPR basalts is less than 1 which is characteristic of asthenosphere-derived magmas. Finally,

429 many alkaline OIB, such as St. Helena-type basalts (Chaffey et al., 1989; Kawabata et al.,

430 2011) show negative K-anomalies, typically those formed by low-degree melting. Although,

431 melting of metasomatized lithosphere cannot be excluded as a potential origin of such basalts

432 (Pilet et al., 2005; 2008), most authors consider them as derived from upwelling hot mantle

433 beneath the oceanic lithosphere. Thus, this compositional feature could be rather general both

434 in oceanic and continental realms and could be an inheritance in the mantle source regions,

435 possibly representing the most fusible part (eclogite or pyroxenite with negative K-anomaly

436 and HIMU/FOZO characteristics; Sobolev et al., 2005; 2007; Fekiacova et al., 2007;

437 Dasgupta et al., 2010; Timm et al., 2009) of the melted mantle material. In this context, it is

438 noteworthy, that a correlation between the K/K* value and the radiogenic isotope ratios

439 ($^{87}Sr/^{86}Sr$ and $^{143}Nd/^{144}Nd$; Fig. 5) is observed within the volcanic fields and that can be more

440 readily explained by derivation of the magmas with compositionally distinct mantle sources.

441 Lower degrees of melting would produce magmas from the more fusible parts of the source

442 region that are characterized by low $^{87}Sr/^{86}Sr$ and high $^{143}Nd/^{144}Nd$ isotope ratios similar to

443 HIMU/FOZO (Stracke et al., 2005) and negative K-anomaly (low K/K*), whereas higher

444 degree of melting would lead to mixing with melts coming from compositionally distinct

445 mantle domains (Harangi and Lenkey, 2007).

446   In summary, derivation of the basaltic magmas solely from the lithospheric mantle

447 does not seem to be a plausible model in the CPR. In turn, we suggest that composition of the

448 CPR basalts is consistent with melting predominantly or even entirely of the asthenospheric

449 mantle. Since there are no convincing evidences for the existence of mantle plume or plume

450 fingers beneath this region, nor progressive lithospheric extension, we think that it is

451 physically difficult to generate significant amount of alkaline sodic magmas in the lithosphere

452 during the post-rift and tectonic inversion stages unless considering local detachment and

453 sinking of lithospheric fragments into the asthenosphere (Timm et al., 2010). At this stage, we

454 think that composition of the CPR basaltic rocks reflects mostly the nature of the source

455 region of the asthenospheric mantle and the heterogeneity within it.

456

457 *Constrains on melting columns*

458

459   Considering that the basaltic magmas in the CPR could derive predominantly from the

460 asthenospheric mantle, an upward mantle flow is required to initiate melting. As the solid

461 mantle material moves upwards adiabatically, melting starts when the ambient temperature

462 intersects the solidus (initial melting pressure; Langmuir et al., 1992). This depth depends on

463 the mantle potential temperature as well as the nature of the mantle material (Langmuir and

464 Forsyth, 2007), but for alkaline mafic magmas it is usually within the garnet stability field, i.e.

465 deeper than 80 km (Niu et al., 2011). Melt production continues during further upwelling and

466 as a result, the initial magma composition will change due to the increasing extent of melting

467 and according to the changing mineral assemblage of the melted mantle rocks (from garnet to

468 spinel). Thus, the early-stage melt shows strong garnet-signature (high Ce/Y, Nb/Y and

469 $[Sm/Yb]_N$ ratios; Ellam, 1992; Salters and Hart; 1989; Putirka, 1999; Niu et al., 2011), but it

470 becomes progressively diluted in the strongly incompatible elements and looses their garnet

471 fingerprint. The extent of the melting column (defined by the initial and final melting

472 pressure, denoted as p_o and p_f, respectively) depends primarily on the thickness of the

473   lithosphere (Ellam, 1992; Langmuir et al., 1992; Haase, 1996; Putirka, 1999; Niu et al., 2011).

474   Melting beneath thick lithosphere stops at greater depth and therefore produces smaller

475   amount of magma, which are enriched in strongly incompatible trace elements and have a

476   pronounced garnet-signature, whereas in areas where the lithosphere is thinner, melting could

477   continue even in the spinel-stability field and produces more melt with different incompatible

478   element abundances. Thus, the p_f can be used as a proxy for the thickness of the lithosphere,

479   i.e. defining the depth of the lithosphere-asthenosphere boundary (LAB).

480   The pressure of the melting can be constrained by various methods. Major element

481   composition of the primitive magmas is influenced by the pressure of melting and the extent

482   of melting (Takahashi and Kushiro, 1983; Langmuir et al., 1992; Hirose and Kushiro, 1993;

483   Baker and Stolper, 1994; Walter, 1998; Niu et al., 2011). MgO and FeO^t increase, SiO_2

484   decreases with increasing pressure of melting, whereas the Na_2O content of the primary

485   magma depends mostly on the degree of melting. The CPR basalts have a relatively wide

486   range of FeO content (FeO^t=8-12 wt%; Fig. 3) showing an inverse correlation with SiO_2

487   indicating that the primary magmas could have formed at various pressures. In order to

488   quantify the pressure of melting, i.e. the depth of the magma generation first, correction of

489   fractional crystallization has to be performed. This can be achieved by adding as much olivine

490   to the bulk rock composition until the mg-number is around 0.72, consistent with a primitive

491   melt composition that is in equilibrium with a melted peridotite with olivine having Fo-

492   content around 0.9 mol%. For the selected mafic rocks of the CPR, correction of 5-15%

493   olivine fractionation was necessary.

494   Langmuir et al. (1992) developed a model where the FeO^t and Na_2O contents of the

495   primary magmas are used to constrain the intitial and final pressure of melting. Although this

496   was constructed for mid-ocean ridge basalts, Wang et al. (2002) demonstrated that it provides

497   reliable results for most melting within the depth interval of 50 and 110 km. The melting

498 model lines were compared with experimentally determined peridotite melts and a good

499 reproduction was obtained between 1.0 and 4.0 GPa. Furthermore, Wang et al. (2002)

500 emphasized that for magmas having $Na_2O>3$ wt% that is relevant for the CPR basalts, the

501 model is not dependant upon the melt pooling mechanism. We used this model calculation,

502 considering accumulated fractional melting process to determine the melting columns under

503 the alkaline basalt volcanic field of the CPR. In the Fig. 6A, each curve represents a different

504 initial melting pressure, i.e. where the ambient mantle temperature intersects the solidus. The

505 total iron content of the magma reflects the condition of the onset of melting, i.e. the initial

506 pressure that has a close relationship also with the mantle temperature. As melting proceeds,

507 the volume of magma increases and as a consequence the concentration of incompatible

508 elements as well as Na_2O decreases, while the total iron concentration does not change

509 significantly. Therefore, the final values of the FeO^t and the Na_2O of the accumulated melt

510 yield information on the initial melting pressure and the cessation of the melting, i.e. the final

511 melting pressure. These pressure values are then converted to depth, assuming average

512 densities of crust and mantle, 2.85 g/cm^3 and 3.25 g/cm^3, respectively as suggested by Wang

513 et al. (2002). The crustal thickness was taken as 32 km beneath Burgenland (western CPR)

514 and 35 km beneath Perşani (eastern CPR), whereas 28 km was used for the rest of the areas.

515 Note that the pressure/depth estimate has an about 10-20 km uncertainty due to various effects

516 such as the estimate of the primary composition, mantle fertility and the neglecting Fe^{3+} in the

517 iron content of the primitive melts (Wang et al., 2002).

518   We obtained p_o and p_f values for 13 basalt localities that cover all the monogenetic

519 volcanic fields of the CPR (Fig. 6A). Within them, only one basalt group from the Nógrád-

520 Gemer Volcanic Field shows a melting column with a depth interval that seems to be

521 unusually shallow (2.0 to 1.55 GPa, i.e. melting between 66 and 52 km). In all other cases the

522 initial and final melting pressure values are greater then 2 GPa; thus, considering the

21

523 lithospheric thickness beneath the Pannonoan basin, they indicate magma generation in the

524 sublithospheric mantle. Generation of the primary magmas started predominantly at around 3

525 GPa, i.e. at 100 km depth. This corresponds with a depth of the spinel-garnet transitional field

526 (Robinson and Wood, 1998; Klemme and O'Neill, 2000; Klemme, 2004). At such depth, dry

527 peridotite could not melt up to a mantle potential temperature of 1450°C, therefore presence

528 of water or pyroxenite/eclogite with lower solidus is expected in the source region that may

529 lead to lower the calculated pressure (Wang et al., 2002). Nevertheless, the final depth of

530 melting columns of the CPR basalts is between 2.1 and 2.5 GPa (70-83 km depth), what is in

531 good agreement with the geophysically determined thickness of the lithosphere (Horváth et

532 al., 2006) beneath the volcanic fields (Fig. 7). In addition to the usual melting depth of the

533 CPR basalts, the alkaline basalts from Burgenland (Pauliberg and Oberpullendorf) fall into the

534 3.4 and 3.8 GPa melting lines (Fig. 6A) that corresponds with an onset of melting at greater

535 depth (110-125 km). This fits, however, well with the deep structure beneath these basaltic

536 volcanoes, i.e. they are located in an area characterized by thick lithosphere (ca. 110 km

537 present day thickness; Fig. 7). The relatively shallow melting column beneath the Perşani

538 volcanic field (86-70 km depth interval) seems to be remarkable, since formerly Dérerova et

539 al. (2006) and Horváth et al. (2006) suggested a thick lithosphere here (about 140 km).

540 However, Harangi et al. (2013) pointed out that the Perşani basaltic magmas were originated

541 by melting of asthenospheric mantle and therefore the LAB should be much shallower, i.e. not

542 deeper than 60 km. This is consistent with the geophysical result of Martin et al. (2006) and

543 implies that a narrow rupture could have developed in the lower lithosphere beneath the

544 Perşani area, probably as a result of the dragging effect of the descending dense lithospheric

545 slab beneath the Vrancea zone located about 100 km from the volcanic field (Harangi et al.,

546 2013). In two cases (Putikov vŕšok and Lucaret), we got a melting column fairly deep in

547 comparison with the lithospheric thickness. Partial melting could start here deeper than 100

548   km and terminated shortly after 10-15 km mantle upwelling. A possible explanation for this

549   would be the exhaustion of the fusible material such as hydrous peridotite or garnet-

550   pyroxenite/eclogite.

551   An independent test of the result provided by the Langmuir et al. (1992) model can be

552   achieved with comparison of the primary magma compositions of the CPR basalts with

553   experimental data sets (Sakuyama et al., 2009) and using other geobarometric calculations

554   (Scarrow and Cox, 1995; Lee et al., 2009). Sakuyama et al. (2009) compiled results of various

555   melting experiments and suggested that SiO_2 content of the primary melt is the most sensitive

556   parameter on melting pressure in the range of 1.0-3.0 GPa and it does not depend significantly

557   on the degree of melting, the initial bulk composition and modal mineralogy. Water content of

558   the source peridotite could slightly increase the SiO_2 content of the melt at constant pressure

559   (Hirose and Kawanoto, 1995) that may lead to slight underestimation of the pressure if dry

560   peridotite melting is considered. Plotting the primary magma compositions of the CPR basalts

561   on the ol'-ne'-qtz' triangular diagram along with the isobaric melting lines as determined by

562   Sakuyama et al. (2009) based on experimental data sets, 2.5-3.5 GPa melting pressures are

563   obtained (Fig. 6B) that are in good agreement with the constrains on the melting columns

564   described above, particularly with the initial melting pressure. The only exception is the

565   basalts from Lucaret for which we got melting pressure of 2.5 GPa, significantly lower than

566   from the Langmuir et al. (1992) model (3.20-2.75 GPa). Scarrow and Cox (1995) developed a

567   simple equation for the melting pressure estimate based on the SiO_2 content of primary rocks.

568   It gives slightly lower pressure values than the ol'-ne'-qtz' diagram, whereas the corrected

569   SiO_2-geobaromether by Wang et al. (2002) appears to strongly overestimate the pressure

570   particularly at higher pressure (>2.5 GPa). Finally, we applied also the peridotite-melt

571   barometer of Lee et al. (2009), which gives consistent result with the SiO_2-barometer of

572   Scarrow and Cox (1995), but also with the final pressure estimate of the Langmuir et al.

573   (1992) model (Fig. 8). There is also a good correlation between the pressure obtained by the

574   Lee et al. (2009) barometry and the qtz'/(ol'-ne'-qtz') ratio, which was suggested as a

575   sensitive parameter of depth of melting (Sakuyama et al., 2009). The only exception is the

576   basalts from Pauliberg that form a parallel trend at slightly higher pressure range, probably

577   due to the difference of the source lithology.

578   In summary, we can conclude that melting of the upwelling asthenospheric mantle

579   material could start at about 100 km depth beneath most of the volcanic fields of the CPR and

580   the final melting pressure could have been controlled by the thickness of the lithosphere, i.e.

581   the lithosphere-asthenosphere boundary. Partial melting occurred at greater depth beneath

582   Pauliberg, which is underlain by thicker lithosphere, whereas beneath the Perşani area melting

583   could have taken place at shallower depth due to a local rupture of the lower lithosphere. The

584   youngest basalt beneath Putikov vŕšok generated at greater depth (100-120 km), whereas the

585   2.4 Ma Lucaret basalt could have been derived also from a relatively shallow depth in spite of

586   the higher FeO content of the basalts.

587

588   ***Conditions of melt generation***

589

590   We proposed that partial melting of the upwelling asthenospheric mantle material

591   could lead to the generation of basaltic magmas, which fed the volcanic eruptions in the

592   monogenetic volcanic fields of the CPR. A further constrain on the melt generation process

593   can be obtained from trace element petrogenetic modelling (Fig. 9). We used different initial

594   compositions (depleted MORB mantle and slightly enriched primitive mantle; Salters and

595   Stracke, 2004; McDonough and Sun, 1995) and different mineralogical assemblage (garnet-

596   lherzolite, spinel lherzolite) of the source material and different melting models (batch and

597   fractional melting; Shaw, 1970; critical or dynamic melting; Sobolev and Shimizu, 1992; Zou,

598   1998; Shaw, 2000) with the mineral-melt distribution coefficients proposed by Kostopoulos

599   and James (1992). Trace element ratios of Zr/Nb and La/Y were chosen, because their values

600   are not dependant on early-stage crystal fractionation and are sensitive (La/Y) on the presence

601   of spinel and garnet in the mantle source. As we discussed earlier, it is unlikely that

602   amphibole was also present in the source region of the CPR basalts and therefore, it was not

603   considered in the modelling calculations. The result of the petrogenetic modelling is shown in

604   Figure 9.

605   The primary magmas of the CPR basalts were formed from trace element enriched

606   mantle source (1.5-4.0-times of the primitive mantle composition; McDonough and Sun,

607   1995) within the spinel-garnet transitional zone (Fig. 9.). The degree of melting is somewhat

608   model dependant, but it is between 1.5% and 5%. The best fit of the CPR basalts with the

609   melting model lines is given assuming continuous dynamic melting or decompressional

610   critical melting (Sobolev and Shimizu, 1992; Zou, 1998; Shaw, 2000) process. This model is

611   consistent with the melting process described in the previous section, i.e. commencing of

612   melting in a mantle source, where garnet prevails over spinel and then continues in the spinel

613   stability field. In this case, 2-3% melting is required to obtain the composition of the primary

614   basaltic magmas of the CPR. Noteworthy, the Lucaret basalts fall on the spinel-peridotite

615   melting line implying shallow melting and suggest that the FeO content of the bulk rock

616   overestimates the melting pressure and the SiO_2-based geobarometries provide more reliable

617   result. On the other hand, the basalts from the western Pannonian Basin (Pauliberg,

618   Oberpullendorf and Klöch from the Styrian basin) fall on the garnet-peridotite melting line

619   consistent with their derivation from a deeper source.

620   The depth of melting for the CPR basalts as shown by various models is between 60

621   and 120 km. The associating melting temperature can be determined using the peridotite-melt

622   thermometer by Lee et al. (2009; using molar $Fe^{3+}/Fe^{tot}=0.13$) and the PRIMELT2 software of

25

623   Herzberg and Asimow (2008; using $Fe_2O_3 = TiO_2$). They resulted in fairly similar temperature

624   values up to 1470^oC (Fig. 7), where the Lee et al. (2009) calculation tends to give much

625   higher ($>100^oC$) temperature than the PRIMELT2 (mostly for the Pauliberg basalts). The

626   lowest mantle potential temperature is shown by the Perşani basalts ($1310\text{-}1380^oC$) that

627   records indeed shallow melting as indicated by the geobarometric calculations, whereas in the

628   other volcanic fields, we got melting temperature in a range between 1350 and 1450^oC. The

629   highest potential temperature values were obtained for the basalts at Pauliberg ($>1440^oC$) and

630   at Putikov vŕšok ($1420\text{-}1450^oC$).

631   Taken together the obtained pressure and temperature values, the Figure 10 shows that

632   the melting columns of the basaltic magmas of the CPR are just below the dry peridotite

633   solidus. This requires either some water or a more fusible material, such as pyroxenite or

634   eclogite in the mantle source. The relatively low CaO content (<10 wt%) of the calculated

635   primary basaltic magmas as well as the low Ca also in the olivine phenocrysts (Harangi et al.,

636   2013) are features that can be explained by pyroxenite melting (Herzberg, 2011). However,

637   the olivine in the CPR basalts (Embey-Isztin and Dobosi, 2007; Jankovics et al., 2012; 2013;

638   Harangi et al., 2013) has relatively low Ni and high Mn concentrations that is just the opposite

639   of what required in the case of pyroxenite melting (Sobolev et al., 2007). These features could

640   be explained, however, also by the lid-effect, i.e. by variations in lithospheric thickness (Niu

641   et al., 2011). Magmas generated under a thin lithosphere could crystallize olivines with

642   relatively low Ni and high Mn and corresponding low Ni/Mg, low Ni/(Mg/Fe) and high

643   Mn/Fe and high Ca/Fe ratios. Although the Ca deficiency of the olivine and the host rocks of

644   the CPR is still unresolved, it appears that the basaltic magmas beneath the CPR could have

645   originated dominantly from a peridotitic mantle source. In this case, however, some water

646   (50-200 ppm; Hirschmann et al., 2009) should be present in the source region. The origin of

647   this volatile content can be explained either by the supposed intense Palaeogene-Miocene

648   subduction around the Carpathians (Csontos et al., 1992) or dewatering of the accumulated

649   subducted material in the transitional zone (Hetényi et al., 2009). An important point coming

650   from the Figure 10. is that the upper mantle beneath the thin continental lithosphere of the

651   Pannonian basin has a temperature close to the peridotite solidus and the mantle could be

652   partially hydrous that makes it potentially still fusible. Eruptions of basaltic magmas in the

653   last 2 Ma could confirm the potentially fusible state of the mantle. The low seismic velocity

654   anomaly down to the transitional zone beneath the northern part of the Pannonian basin

655   (Dando et al., 2011) could provide a further supporting evidence of this.

656

657   *Mantle source characteristics*

658

659   Chromian spinels enclosed by olivine phenocrysts could provide important

660   information about the mantle sources of the CPR basalts. They occur in each volcanic field

661   and therefore it can be used to gain insights into the nature of the sublithospheric mantle on a

662   regional scale. Chromian spinel is often the liquidus phase along with olivine in basaltic melts

663   (Fisk and Bence, 1980; Luhr and Carmichael, 1985), therefore it reflects the primary

664   characteristics of the basaltic melt. It can be used for deciphering the original magmatic

665   characteristics even of heavily altered basalts (Allan, 1992). Composition of the liquidus

666   spinels is considered to be close to that of the spinels in the residual mantle source region,

667   although other controlling factors such as magma differentiation, crystallization pressure,

668   redox condition and the degree of partial melting also influence the composition of spinels

669   (Hill and Roeder, 1974; Sigurdsson and Schilling, 1976; Dick and Bullen, 1984; Allan et al.,

670   1988; Roeder and Reynolds, 1991; Arai, 1994; Clynne and Borg, 1997; Kamenetsky et al.,

671   2001; Roeder et al., 2003).

672   The spinel inclusions found in the CPR basalts show a wide compositional range (cr-

673   number=0.15-0.68, mg-number=0.2-0.8). They are mostly chromian spinels thought to be

674   formed as early-stage mineral phases, however, as soon as they became out of the narrow

675   temperature interval where they could appear as liquidus crystals (Sigurdsson and Schilling,

676   1976; Fisk and Bence, 1980; Luhr and Carmichael, 1985), they react with the differentiated

677   melt and the spinel component is rapidly replaced by magnetite and ulvöspinel components

678   increasing their FeO and Fe_2O_3, and TiO_2 contents (Luhr and Carmichael, 1985; Clynne and

679   Borg, 1997; Arai, 1992; Roeder et al., 2003). Therefore, we selected spinels enclosed by the

680   most magnesian (Fo>84 mol%) olivines and then, we filtered out the analyzed spinel

681   compositions using their TiO_2 and Fe^{3+}-number in order to focus on the most primitive spinel

682   population. Instead of using a definite limit of these parameters (e.g., Clynne and Borg, 1987),

683   we plot all the data on the Cr-Fe^{3+}-Al triangular diagram and compared them with the natural

684   basalt-hosted spinel compositional range (Barnes and Roeder, 2001). The majority of the

685   MORB spinels show a wide variation in the Cr-Al trend, whereas many spinels from OIB

686   have a slight enrichment in Ti and Fe. We selected the spinel population thought to represent

687   liquidus mineral phases primarily based on the overlap with the 50th percentiles of the OIB

688   and MORB spinels and then we considered the possible differentiation trends. The whole data

689   set and the selected "liquidus-spinel" compositions are shown in Fig. 11. The primary spinels

690   form four coherent groups in the Cr-Fe^{3+}-Al diagram that could represent different mantle

691   domains beneath the CPR. Three of them appear in all major volcanic fields of the CPR,

692   whereas the forth one belongs solely to the Pauliberg location. In general, spinel composition

693   closely mimics the host rock composition (as shown by the correlation between the cr-number

694   of spinels and the $Fe_2O_3^t$, Al_2O_3 and TiO_2 contents of the host rock). The basanites of

695   Pauliberg have a specific composition within the Miocene-Quaternary alkaline basalts of the

696   CPR (Embey-Isztin and Dobosi, 1995; Ali and Ntaflos, 2011) showing depletion in Al and

697   enrichment in Fe and Ti compared with the others. Spinels in these rocks are also depleted in

698   Al (thus, they have relatively high cr-number) and slightly enriched in Fe and Ti, plotting

699   outside from the MORB and OIB spinel fields. Nevertheless, considering the specific

700   composition of their host rock, they could also belong to the "liquidus-spinel" population and

701   reflect a particular mantle source region of the Pauliberg magmas. Tentatively, this might be a

702   sign of involvement of eclogite during melting, a hypothesis that requires further studies.

703   Compositional characters of the spinels are controlled by many factors as listed before.

704   Influence of the magma differentiation could be filtered out by limiting the data set to the

705   most primitive spinels. The pressure of crystallization affects predominantly the Al content of

706   the chromian spinels (Dick and Bullen, 1984) showing positive correlation between them. The

707   large compositional variation of the spinel compositions in the CPR basalts, however, could

708   be unlikely related to the variable crystallization pressures, since the lowest Al content in

709   spinels was recorded in those basalts which were interpreted as derived from the deepest

710   source (Pauliberg, Putikov, Lucaret). Spinel composition is dependant also on the degree of

711   partial melting as demonstrated by Arai (1994) and Baker and Stolper (1994). The cr-number

712   of spinel in the mantle restite rock increases with increasing degree of melting. Spinels with

713   0.10-0.15 cr-number are considered to represent fertile mantle regions, whereas spinels with

714   cr-number of about 0.6 could indicate more than 25% degree of melting (Baker and Stolper

715   1994). However, no correlation can be recognized between the variation of spinel cr-number

716   and the incompatible trace element ratios of the CPR basalts that are sensitive on the

717   progressive melting process (e.g., La/Y, $[Sm/Yb]_N$). Furthermore, our petrogenetic model

718   calculation suggests that the mafic magmas of CPR could have originated by 2-3% of melting

719   and therefore, the large compositional variation of spinels cannot be attributed to various

720   degrees os partial melting. Taking all of these into account, we can conclude that the spinels

721   in the CPR basalts reflect the nature of the mantle source region, more precisely the character

722   of the residual mantle rocks and indicates heterogeneous, variably depleted sublithospheric

723   mantle beneath the Pannonian basin.

724   Spinel compositions suggest that at least three main compositional domains (and a

725   specific one beneath Pauliberg) could exist in the mantle source region and they are well

726   distributed beneath each volcanic field. Although the composition of the liquidus spinels is

727   close to the spinels in the restitic mantle rocks rather than in the intitial source material, the

728   small degree of melting characterizing the CPR basalts could not significantly modify the

729   compositional feature of the intial spinels as also emphasized by Clynne and Borg (1997) for

730   the Lassen basalts. Therefore, the composition of the restite spinels could be close to that of

731   the initial ones. Noteworthy, the youngest (<600 ka) basalts could have derived either from

732   the most fertile mantle source domain (Perşani basalts; spinel cr-number=0.23-0.32; Harangi

733   et al., 2013) or from a mantle domain akin to enriched OIB (Putikov vŕšok; spinel cr-

734   number=0.55-0.61; TiO_2=2.0-3.5 wt%; Sági et al., in prep). This might mean that the

735   sublithospheric mantle beneath CPR could be potentially still capable to produce basaltic

736   magmas, i.e. contains fusible parts of material.

737

738   *Geodynamic relationships*

739

740   The origin of the alkaline basaltic volcanism in the CPR seems to be enigmatic since it

741   occurred after the main phase of the lithospheric extension of the Pannonian basin (20-15 Ma;

742   Horváth et al., 2006), during the stage of post-rift thermal subsidence and tectonic inversion.

743   Melt generation has taken place intermittently since 11 Ma with a peak period between 5 and

744   1 Ma. In such situations, hot mantle upwelling beneath the thinned lithospheric realm seems

745   to be a viable mechanism to produce low-volume basaltic magma (Embey-Isztin et al., 2001;

746   Harangi, 2001b). Composition of the Neogene alkaline mafic rocks in Europe shares many

747 similarities, particularly in the radiogenic isotope ratios. Taking this into account and

748 correlating it with seismic anomalies in the sublithospheric mantle beneath Europe, Hoernle et

749 al. (1995) and Granet et al. (1995) proposed a common mantle reservoir of the mafic magmas

750 (called European Asthenospheric Reservoir; EAR by Cebriá and Wilson, 1995) that fed the

751 basaltic volcanism via localized active mantle plumes ("plume finger") in different parts of

752 Europe, such as in the Massif Central, the Rhenish area, the Eger graben, Bohemia and also in

753 the Pannonian basin (Granet et al., 1995; Wilson and Patterson, 2001). The plume finger

754 model was put forward for the Pannonian basin by Embey-Isztin et al. (2001), Seghedi et al.

755 (2004b) and Seghedi and Downes (2011). Seghedi et al. (2004b) distinshuished at least three

756 plume fingers beneath the CPR, primarily based on the HIMU-like isotopic character of the

757 basalts. However, we have to emphasize that the HIMU-like isotopic ratios have solely a

758 descriptive message and this does not necessarily mean plume-origin. Nevertheless, the

759 plume-related basaltic magmatism in the CPR was proposed also by other authors based on

760 geological, geochemical and geophysical considerations (Goes et al., 1999; Buikin et al.,

761 2005; Burov and Cloetingh, 2009). In contrast, Harangi and Lenkey (2007) argued against a

762 mantle plume beneath the Pannonian basin.

763   There are a couple of observations that are not consistent with the plume model.

764 Beneath the Pannonian basin, in the depth range of 400-650 km, a positive seismic velocity

765 anomaly is recognized (Wortel and Spakman, 2000; Piromallo et al., 2001; Piromallo and

766 Morelli, 2003; Hetényi et al. 2009). The origin of this anomaly was postulated as

767 accumulation of thick, cold material, possibly subducted residual material supplied from

768 several subduction episodes (Penninic in the Cretaceous, Vardar in the Palaeogene, and the

769 East Carpathian subduction in the Miocene; Hetényi et al. 2009). This vast amount of cold

770 material can form a barrier against the rise of any lower mantle-derived plume and prevents

771 the initiation of upwelling of hot material from the Transition Zone. However, it has been

31

772   shown that the Transitional Zone could be one of the wettest parts of the upper mantle,

773   particularly when subducted material is accumulated there for a long time (Hirschmann, 2006;

774   Karato, 2011). Thus, it could serve as the source for wet plumes instead of hot plumes. In this

775   scenario, wet melting in the upper part of the Transition Zone (Hirschmann, 2006) could

776   provide small volume hydrous magmas that initiate further melting beneath the continental

777   lithosphere. Although this is a reasonable scenario it does not explain the observation why the

778   basaltic volcanic fields are at the marginal parts of the Pannonian basin and not in the central

779   areas. The characteristic features of hot mantle plumes are also missing in the CPR. The broad

780   topographic updoming such as detected in the Massif Central (Wilson and Patterson, 2001), or

781   in classic hot spot areas (Courtillot et al., 2003), is absent; on the contrary, some parts of the

782   Pannonian Basin are still subsiding. The high heat flow in the CPR (Lenkey et al., 2002) can

783   be readily explained by the thinning of the lithosphere during basin formation and by the still

784   shallow asthenosphere (Royden et al., 1982). As far as the HIMU-like isotopic ratios of some

785   CPR basalts are concerned, they could have also a metasomatic origin (e.g., Hart, 1988; Sun

786   and McDonough, 1989; Halliday et al., 1995; Pilet et al., 2005). The sporadic distribution and

787   the low-magma output type of the volcanic fields in the CPR also do not support any hot

788   mantle plume origin. Therefore, there are no supporting evidences that favour hot mantle

789   plume or plume finger (Seghedi et al., 2004) origin of the basaltic volcanism in the CPR.

790   Generation of basaltic magmas in the asthenosphere requires upward movement of

791   solid mantle material, i.e. a mantle flow. In this context, the spatial distribution of the basalt

792   volcanic fields at the peripheral areas of the CPR could have relevance. They occur above a

793   lithosphere-asthenosphere boundary with sharp depth variation between the orogenic Alps

794   and cratonic North European Platform with thick (>160 km) lithospheric roots and the

795   stretched Pannonian basin with thin (< 70 km) lithosphere within relatively short distances

796   (Fig. 12.). The Pannonian basin could therefore act as a thin-spot providing suction in the

32

797 sublithospheric mantle and generating mantle flow from below the thick lithospheric roots

798 (Harangi and Lenkey, 2007; Harangi, 2009). The SKS splitting measurements show a

799 dominant west-east direction beneath the western part of the Pannonian basin with a clear

800 continuation from the Alps and this direction changes to a northwest-southeast trend toward

801 the central and northern areas (Kovács et al. 2012). On the western side of the Alps, similar,

802 east-west directed SKS splitting directions were recognized that turn gradually in north-south

803 direction northward and this was considered as relatively recent asthenospheric flow (Barroul

804 et al. 2011). Remarkably, a similar seismic pattern was observed also in the Lake Baikal area,

805 where it was interpreted as sublithospheric mantle flow from beneath the thick Siberian craton

806 towards the thin Baikal–Mongolian area (Lebedev et al., 2006). The low-volume, scattered,

807 and sporadic basalt volcanism in the Baikal rift could have been connected with this mantle

808 flow by decompression melting when the asthenospheric material ascended from the 200-km

809 depth beneath the craton to shallower depths beneath the rift (Lebedev et al., 2006). A similar

810 triggering mechanism was put forward by Niu (2005) explaining the basaltic volcanism in the

811 East China lowland. Thus, it appears that a large contrast in the LAB architecture could

812 enhance mantle flow that results in intraplate basaltic volcanism with many similarities to

813 OIB-type compositions. This appears to be the case also in the Alps-Pannonian basin

814 transition zone, where relatively hot asthenospheric material could ascend from beneath the

815 Alps along the steep LAB (Harangi, 2009; Fig. 13). The important role of asthenospheric

816 mantle flow as a driving force for the Neogene extension and extrusion events is getting to

817 have an increasing attention in the geodynamic model of the Pannonian basin. Konečný et al.

818 (2002) invoked an asthenospheric flow due to subduction roll-back mechanism and explained

819 the magma generation by this process. Kovács et al. (2012) proposed that this mantle flow is

820 the result of the convergence between the Eurasian and African plates along the Alpine belt,

821 whereas Horváth and Faccenna (2011) suggested that mantle material was pumped through

822   the Istria slab window beneath the CPR mantle as a result of slab rollback along the eastern

823   margin of the region. An important difference between these models and the explanation put

824   forward in this paper is the time of the mantle flow. According to Konečný et al. (2002),

825   Kovács et al. (2012) and Horváth and Faccenna (2011) this process could have been taking

826   place since the Oligocene/Miocene and act as a major role in the geodynamic evolution of the

827   CPR, whereas here, we propose that it is a passive process commenced just after the Mid-

828   Miocene formation of the Pannonian basin with strongly thinned lithosphere and in this case

829   this thin spot condition acted as a driving force of the mantle flow.

830   In the northern part of the Pannonian basin, there has been a long lasting volcanic

831   activity since about 16 Ma (Harangi et al., 2007). The alkaline basalt volcanism followed an

832   intense calc-alkaline volcanic period (Konečný et al., 1995; 2002). Nevertheless, no traces of

833   subduction-related mantle source are observed in the composition of the basaltic products. It

834   can be explained by effective change in the sublithospheric mantle beneath the Štiavnica and

835   Nógrád-Gemer area that could require again mantle flow mechanism. In the seismic

836   tomography model sections published by Dando et al. (2011) a low-velocity anomaly can be

837   observed beneath this region that has a continuation into the deeper mantle towards north.

838   Tentatively, this can be interpreted as a sign of an upward flow beneath the steep LAB. The

839   low magma output and the sporadic eruption events over several million years long period (8-

840   0.1 Ma) could suggest, however, a tectonic control of the melt generation-magma ascent

841   processes. Strain localization in the upper mantle beneath major faults that penetrate the upper

842   mantle (Leloup et al. 1995; Vauchez et al., 2012) could be a possible mechanism of this.

843   Reactivation of transtensional tectonic lines could have a close link with the tectonic inversion

844   of the Pannonian basin (Horváth and Cloetingh, 1996) that started in the Late Miocene when

845   the peak magma-output phase occurred in the Bakony-Balaton Upland and the Štiavnica and

846   Nógrád-Gemer volcanic fields. Further research could focus on the interrelationship of

847   tectonic processes along pre-existing lines and the volcanic events.

848   The youngest basalt volcanic field was developed at the eastern part of the CPR

849   (Perşani area; Seghedi and Szakács, 1994; Downes et al., 1995) from 1.2 to 0.6 Ma (Panaiotu

850   et al., 2013). Seghedi et al. (2011) invoked toroidal asthenospheric flow around the

851   downgoing slab beneath Vrancea to explain the localized alkali basalt volcanism, whereas

852   Harangi et al. (2013) proposed that this could have occurred as a response to the formation of

853   a narrow rupture in the lower lithosphere, possibly as a far-field effect of the dipping of dense

854   continental lithospheric material beneath the Vrancea zone. Upper crustal extensional stress

855   field with reactivation of normal faults at the eastern margin of the Transylvanian basin could

856   enhance the rapid ascent of the mafic magmas.

857   Finally, it is remarkable that local low-velocity mantle anomaly has been detected

858   beneath both the Štiavnica and the Perşani areas (Dando et al., 2011; Popa et al., 2012) that

859   along with our interpretation about the presence of mantle region containing still fusible

860   material suggest that further volcanic eruptions cannot be unambiguously excluded in these

861   areas. The rapid ascent of the magmas (Harangi et al., 2013; Jankovics et al., 2013) implies

862   that the quiet situation could change rapidly.

863

864   **Summary**

865

866   Evaluation of the major and trace element content of the most primitive basalts in the

867   CPR along with the interpretation of the most primitive spinel compositions indicates that the

868   primary magmas could have generated in the convective asthenosphere. Trace element

869   modelling indicates incompatible trace element-enriched source composition and 2-3%

870   melting within the garnet-spinel transition zone. Melting started at about 100 km depth where

871   garnet prevails over spinel and continued usually up to the base of the lithosphere. Thus, the

872   final melting pressure could indicate the ambient lithosphere-asthenosphere boundary (LAB).

873   The asthenospheric mantle source regions of the basalts were heterogeneous, presumably at

874   small scale. Spinel compositions show a wide range, although four coherent groups can be

875   distinguished that are interpreted as reflect the main mantle domains beneath this region. They

876   can be recognized at almost each volcanic field. Two of these have fertile and slightly

877   depleted character, respectively, whereas the two others are enriched in Fe and Ti and overlap

878   the spinels found in the basalts of Hawaii. They might indicate involvement of

879   pyroxenitic/eclogitic lithology in the melting process that requires further investigation. Major

880   element composition of some of the basalts (low Al and high Ti and Fe; e.g., Pauliberg,

881   Putikov) could be also consistent with melting of carbonated, silica-deficient eclogite. Indeed,

882   considering the depths of the estimated melting columns of the CPR basaltic magmas, a more

883   fusible material than the dry peridotite is required in the source regions of the magmas.

884   Presence of water or pyroxenite/eclogite could explain melting at such depth.

885   The prevailing estimated mantle potential temperature (1300-1400°C) along with

886   number of further observations do not require anomalously hot asthenospheric mantle. Thus,

887   we can exclude the presence of any mantle plume or mantle plume fingers beneath the

888   Pannonian basin. The locations of the monogenetic basalt volcanic fields at the western and

889   northern margin of the Pannonian basin could indicate a close relationship with the steep LAB

890   beneath these areas. We propose that asthenospheric flow from beneath the adjoining thick

891   lithospheric domains (Alps, cratonic North European Platform) to the thinned Pannonian

892   basin could play a triggering role in the melt generation. A near vertical upwelling along the

893   steep LAB could result in decompressional melting producing low-volume melts. The

894   Pannonian basin could therefore act as a thin-spot after the Mid-Miocene syn-rift phase (20-

895   12 Ma) and provided suction in the sublithospheric mantle generating asthenospheric flow

896   from below the thick lithospheric roots. In addition to this dominant process, single basaltic

897   volcanic events in the inner part of the Pannonian basin could have been related to strain-

898   localization in the upper mantle beneath major strike-slip faults that penetrate the upper

899   mantle. Further southeast, close to the Vrancea zone, the youngest basalt volcanic field in the

900   CPR could have been formed as a plate tectonic response of the dipping dense continental

901   lithospheric material. The suction of the descending lithospheric slab could result in narrow

902   rupture at the base of the lithosphere. Decompression melting of the upwelling asthenospheric

903   mantle could result in magma generation, while reactivation of normal faults enhanced the

904   rapid ascent of the magmas.

905   Origin of basaltic magmas with fairly primitive composition for the last 1 Ma implies

906   that fusible material could still exists in the mantle, which have a potential temperature close

907   to the solidus. This inferred condition and the low-velocity anomalies detected in the mantle

908   depths as well as the still high localized heat flows in these areas all suggest that continuation

909   of the basaltic volcanism in the CPR cannot be unambiguously excluded.

910

References

930

931 Aldanmaz E, Koprubasi N, Gurer ÖF, Kaymakci N, Gourgaud A (2006) Geochemical

932   constraints on the Cenozoic, OIB-type alkaline volcanic rocks of NW Turkey:

933   Implications for mantle sources and melting processes. Lithos 86:50-76.

934 Ali S, Ntaflos T (2011) Alkali basalts from Burgenland, Austria: Petrological constraints on

935   the origin of the westernmost magmatism in the Carpathian-Pannonian Region. Lithos,

936   121:176-188

937 Ali S, Ntaflos T, Upton BGJ (2013) Petrogenesis and mantle source characteristics of

938   Quaternary alkaline mafic lavas in the western Carpathian-Pannonian Region, Styria,

939   Austria. Chemical Geology, 337-338:99-113.

940 Allan JF (1992) Cr-spinel as a petrogenetic indicator: deducing magma composition from

941   spinel in highly altered basalts from the Japan Sea, Sites 794 and 797. Proc. Ocean

942   Drilling Program 127/128:837-847.

943 Allan JF, Sack RO, Batiza R (1988) Cr-rich spinels as petrogenetic indicators; MORB-type

944   lavas from the Lamont seamount chain, eastern Pacific. American Mineralogist

945   73:741-753.

946   Arai S (1992) Chemistry of chromian spinel in volcanic rocks as a potential guide to magma

947   chemistry. Mineralogical Magazine 56:173-184.

948   Arai S (1994) Compositional variation of olivine-chromian spinel in Mg-rich magmas as a

949   guide to their residual spinel peridotites. Journal of Volcanology and Geothermal

950   Research, 59:279-293.

951   Bada G, Horváth F, Fejes I, Gerner P (1999) Review of the present-day geodynamics of the

952   Pannonian basin: progress and problems. Journal of Geodynamics, 27:501–527.

953   Baker MB, Stolper EM (1994) Determining the composition of high-pressure mantle melts

954   using diamond aggregates. Geochim. Cosmochim. Acta 58:2811-2827.

955   Balázs E, Nusszer A (1987) Unterpannonischer Vulkanismus der Beckengebiete Ungarns.

956   Annales of Hungarian Geological Institute, 69:95-104.

957   Balogh K, Németh K (2005) Evidence for the Neogene small-volume intracontinental

958   volcanism in the Western Hungary: K/Ar geochronology of the Tihany Maar Volcanic

959   Complex. Geologica Carpathica 56:91–99.

960   Balogh K, Mihalikova A, Vass D (1981) Radiometric dating of basalt in Southern and Central

961   Slovakia. Zap. Karpaty, ser. Geol. 7:113 126.

962   Balogh K, Jámbor A, Partényi Z, Ravaszné Baranyai L, Solti G (1982) A dunántúli bazaltok

963   K/Ar radiometrikus kora. A Magyar Állami Földtani Intézet Évi Jelentése az 1980.

964   évről:243-259.

965   Balogh K, Árva-Sós E, Pécskay Z, Ravasz-Baranyai L, (1986) K/Ar dating of post-Sarmatian

966   alkali basaltic rocks in Hungary. Acta Mineralogica et Petrographica Szeged 28:75-93.

967   Balogh K, Harald L, Pécskay Z, Ravasz Cs, Solti G (1990) K/Ar radiometric dating of the

968   Tertiary volcanic rocks of East-Styria and Burgenland. MÁFI Évi Jel. 1988-ról:451-

969   468.

970   Balogh K, Ebner F, Ravasz Cs (1994) K/Ar alter tertiärer Vulcanite de südöstlischen

971   Steiermark und des südlichen Burgenlands. In: Császár, G, Daurer, A. (Eds.),

972   Jubiläumsschrift 20 Jahre Geologischen Zusammenarbeit Österreich-Ungarn Lobitzer,

973   55–72.

974   Balogh K, Itaya T, Németh K, Martin U, Wijbrans J, Thanh NX (2005) Study of controversial

975   K/Ar and 40Ar/39Ar ages of the Pliocene alkali basalt of Hegyestű, Balaton Highland,

976   Hungary: a progress report. Mineralia Slovaca 37:298–300.

977   Barnes SJ, Roeder PL (2001) The Range of Spinel Compositions in Terrestrial Mafic and

978   Ultramafic Rocks. Journal of Petrology 42:2279-2302.

979   Barruol G, Bonnin M, Pedersen H, Bokelmann GHR, Tiberi C (2011) Belt-parallel mantle

980   flow beneath a halted continental collision: the Western Alps. Earth and Planetary

981   Science Letters, 302:429-438

982   Beccaluva L, Bianchini G, Bonadiman C, Coltorti M, Milani L, Salvini L, Siena F, Tassinari

983   R (2007) Intraplate lithospheric and sub-lithospheric components in the Adriatic

984   domain: Nephelinite to tholeiite magma generation in the Paleogene Veneto Volcanic

985   Province, Southern Alps. In: Beccaluva, L, Bianchini, G, Wilson, M. (Eds.), Cenozoic

986   Volcanism in the Mediterranean Area: Geological Society of America, Special paper,

987   418:131–152.

988   Beccaluva L, Bianchini G, Natali C, Siena F (2011) Geodynamic control on orogenic and

989   anorogenic magmatic phases in Sardinia and Southern Spain: Inferences for the

990   Cenozoic evolution of the western Mediterranean. Lithos, 123:218–224.

991   Bianchini G, Beccaluva L, Siena F (2008) Postcollisional and intraplate Cenozoic volcanism

992   in the rifted Apennines/Adriatic domain. Lithos, 101:125–140.

993   Blondes MS, Reiners PW, Ducea MN, Singer BS, Chesley J (2008) Temporal-compositional

994   trends over short and long time-scales in basalts of the Big Pine Volcanic Field,

995   California. Earth and Planetary Science Letters 269:140-154.

996   Borsy Z, Balogh K, Kozák M, Pécskay Z (1986) Újabb adatok a Tapolcai-medence

997   fejlõdéstörténetéhez. Acta Geographica Debrecina 23:79-104.

998   Bradshaw, TK, Hawkesworth CJ, Gallagher K (1993) Basaltic volcanism in the Southern

999   Basin and Range: no role for a mantle plume. Earth and Planetary Science Letters,

1000   116:45-62.

1001   Brenna M, Cronin SJ, Smith IEM, Sohn YK, Németh K (2010) Mechanisms driving

1002   polymagmatic activity at a monogenetic volcano, Udo, Jeju Island, South Korea.

1003   Contributions to Mineralogy and Petrology 160:931-950.

1004   Brenna M, Cronin SJ, Smith IEM, Maas R, Sohn YK (2012) How small-volume basaltic

1005   magmatic systems develop: a case study from the Jeju Island Volcanic Field, Korea.

1006   Journal of Petrology 53:985-1018.

1007   Buikin A, Trieloff M, Hopp J, Althaus T, Korochantseva E, Schwarz WH, Altherr R (2005)

1008   Noble gas isotopes suggest deep mantle plume source of late Cenozoic mafic alkaline

1009   volcanism in Europe. Earth and Planetary Science Letters, 230:143-162.

1010   Burov E, Cloetingh S (2009) Controls of mantle plumes and lithospheric folding on modes of

1011   intraplate continental tectonics: differences and similarities. Geophysical Journal

1012   International, 178:1691-1722.

1013   Cebriá, JM, Wilson M (1995) Cenozoic mafic magmatism in western/central Europe: A

1014   common European asthenospheric reservoir? Terra Nova, 7:162.

1015   Cebriá JM, López-Ruiz J (1995) Alkali basalts and leucitites in an extensional intracontinental

1016   plate setting: The late Cenozoic Calatrava Volcanic Province (central Spain). Lithos,

1017   35:27-46.

1018 Chaffey DJ, Cliff RA, Wilson BM (1989) Characterization of the St. Helena magma source. –

1019   In: Saunders AD, Norry MJ (Eds) Magmatism in the Ocean Basins. Geological

1020   Society Special Publication, 42:257-276.

1021 Chernyshev IV, Konečný V, Lexa J, Kovalenker VA, Jeleň S, Lebedev VA, Goltsman YV

1022   (2013) K-Ar and Rb-Sr geochronology and evolution of the Štiavnica Stratovolcano

1023   (Central Slovakia). Geologica Carpathica 64: 327-351

1024 Class C, Goldstein SL (1997) Plume–lithosphere interactions in the ocean basins: constraints

1025   from the source mineralogy. Earth and Planetary Science Letters 150:245–260.

1026 Cloetingh SAPL, Ziegler PA, Bogaard PJF, Andriessen PAM, Artemieva IM, Bada G, Balen

1027   RT, Beekman F, Ben-Avraham Z, Brun JP, Bunge HP, Burov EB, Carbonell R,

1028   Facenna C, Friedrich A, Gallart J, Green AG, Heidbach O, Jones AG, Matenco L,

1029   Mosar J, Oncken O, Pascal C, Peters G, Sliaupa S, Soesoo A, Spakman W,

1030   Stephenson RA, Thybo H, Torsvik T, de Vicente G, Wenzel F, Wortel MJR, TOPO-

1031   EUROPE Working Group 2 (2007) TOPO-EUROPE: The geoscience of coupled deep

1032   Earth-surface processes. Global and Planetary Change 58:1-118.

1033 Clynne MA, Borg LE (1997) Olivine and chromian spinel in primitive calc-alkaline and

1034   tholeiitic lavas from the southernmost Cascade Range, California; a reflection of

1035   relative fertility of the source. The Canadian Mineralogist 35:453-472.

1036 Condit CD, Connor CB (1996) Recurrence rates of volcanism in basaltic volcanic fields: An

1037   example from the Springerville volcanic field, Arizona. Geological Society of

1038   America Bulletin, 108:1225–1241

1039 Connor CB, Conway FM (2000) Basaltic Volcanic Fields. in: Sigurdsson H (Ed.)

1040   Encyclopedia of Volcanoes. Academic Press. San Diego pp 331-343.

1041 Courtillot V, Davaille A, Besse J, Stock J (2003) Three distinct types of hotspots in the

1042   Earth's mantle: Earth Planetary Science Letters, 205:295-308.

1043   Csontos L, Nagymarosy A, Horváth F, Kovác M, (1992) Tertiarry evolution of the intra-
1044   Carpathian area: a model. Tectonophysics, 208:221-241

1045   Dando BDE, Stuart GW, Houseman GA, Hegedűs E, Brückl E, Radovanovic S (2011)
1046   Teleseismic tomography of the mantle in the Carpathian-Pannonian region of central
1047   Europe. Geophysical Journal International, 186:11-31.

1048   Dasgupta R, Hirschmann MM, Stalker K (2006) Immiscible transition from carbonate-rich to
1049   silicate-rich melts in the 3 GPa melting interval of eclogite+CO3 and genesis of silica-
1050   undersaturated ocean island lavas. Journal of Petrology 47:647–671.

1051   Dasgupta R, Jackson MG, Lee CTA (2010) Major element chemistry of ocean island basalts -
1052   conditions of mantle melting and heterogeneity of mantle source. Earth and Planetary
1053   Science Letters 289:377-392.

1054   DePaolo DJ, Daley EE (2000) Neodymium isotopes in basalts of the southwest basin and
1055   range and lithospheric thinning during continental extension. Chemical Geology,
1056   169:157-185.

1057   Dérerova J, Zeyen H, Bielik M, Salman K (2006) Application of integrated geophysical
1058   modeling for determination of the continental lithospheric thermal structure in the
1059   eastern Carpathians. Tectonics, 25:TC3009. doi:10.1029/2005TC001883.

1060   Dick HJB, Bullen T (1984) Chromian spinel as a petrogenetic indicator in abyssal and alpine-
1061   type peridotites and spatially associated lavas. Contributions to Mineralogy and
1062   Petrology, 86:54-76.

1063   Dobosi G (1989) Clinopyroxene zoning patterns in the young alkali basalts of Hungary and
1064   their petrogenetic significance. Contributions to Mineralogy and Petrology, 101:112-
1065   121.

1066   Dobosi G, Fodor RV (1992) Magma fractionation, replenishment, and mixing as inferred

1067   from green-core clinopyroxenes in Pliocene basanite, southern Slovakia. Lithos

1068   28:133-150.

1069   Dobosi G, Fodor RV, Goldberg SA (1995) Late-Cenozoic alkali basalt magmatism in

1070   Northern Hungary and Slovakia: petrology, source compositions and relationship to

1071   tectonics. Acta Vulcanologica, 7:199-207.

1072   Dombrádi E, Sokoutis D, Bada G, Cloetingh S, Horváth F (2010) Modelling deformation of

1073   the Pannonian lithosphere: Lithospheric folding and tectonic topography.

1074   Tectonophysics, 484:103-118.

1075   Downes H, Seghedi I, Szakács A, Dobosi G, James DE, Vaselli O, Rigby IJ, Ingram GA, Rex

1076   D, Pécskay Z (1995) Petrology and geochemistry of late Tertiary/Quaternary mafic

1077   alkaline volcanism in Romania. Lithos, 35:65-81.

1078   Ellam RM (1992) Lithospheric thickness as a control on basalt geochemistry. Geology,

1079   20:153-156,

1080   Embey-Isztin A, Dobosi G (1995) Mantle source characteristics for Miocene-Pleistocene

1081   alkali basalts, Carpathian-Pannonian Region: A review of trace elements and isotopic

1082   composition. Acta Vulcanologica, 7:155-166.

1083   Embey-Isztin A, Dobosi G (2007) Composition of olivines in the young alkali basalts and

1084   their peridotite xenoliths from the Pannonian Basin. Annales Historico-Naturales

1085   Musei Nationalis Hungarici 99:5-22.

1086   Embey-Isztin A, Downes H, James DE, Upton BGJ, Dobosi G, Ingram GA, Harmon RS,

1087   Scharbert HG (1993) The petrogenesis of Pliocene alkaline volcanic rocks from the

1088   Pannonian Basin, Eastern Central Europe. Journal of Petrology 34:317-343.

1089   Embey-Isztin A, Dobosi G, Altherr R, Meyer HP (2001) Thermal evolution of the lithosphere

1090   beneath the western Pannonian Basin: evidence from deep-seated xenoliths.

1091   Tectonophysics 331:285-306.

1092   Erlund EJ, Cashman KV, Wallace, PJ, Pioli L, Rosi M, Johnson E, Granados HD (2010)

1093   Compositional evolution of magma from Parícutin Volcano, Mexico: The tephra

1094   record. Journal of Volcanology and Geothermal Research, 197:167-187.

1095   Fekiacova Z, Mertz DF, Hofmann AW (2007) Geodynamic setting of the Tertiary Hocheifel

1096   volcanism (Germany), Part II: Geochemistry and Sr, Nd and Pb isotopic compositions.

1097   In: Ritter J, Christensen U (Eds) Mantle Plumes - A Multidisciplinary Approach,

1098   Springer, pp. 207-239.

1099   Fisk MR, Bence AE (1980) Experimental crystallization of chrome spinel in FAMOUS basalt

1100   527-1-1. Earth and Planetary Science Letters 48:111-123.

1101   Fitton JG, James D, Kempton PD, Ormerod DS, Leeman WP (1988) The Role of Lithospheric

1102   Mantle in the Generation of Late Cenozoic Basic Magmas in the Western United

1103   States. Journal of Petrology Special Volume 1:331-349.

1104   Fitton JG, James D, Leeman WP (1991) Basic magmatism associated with Late Cenozoic

1105   extension in the Western United States: compositional variations in space and time.

1106   Journal of Geophysical Research, 96:13693-13711.

1107   Gazel E, Plank T, Forsyth DW, Bendersky C, Lee C, Hauri E (2012) Lithosphere vs.

1108   asthenosphere mantle sources at Big Pine Volcanic Field. Geochemistry, Geophysics,

1109   Geosystems, 13:doi:10.1029/2012GC004060

1110   Gîrbacea R, Frisch W (1998) Slab in the wrong place: Lower lithospheric mantle

1111   delamination in the last stage of Eastern Carpathians subduction retreat. Geology,

1112   26:611-614.

1113   Goes S, Spakman W, Bijwaard H (1999) A lower mantle source for central European

1114   volcanism, Science, 286:1928-1931.

1115   Granet M, Wilson M, Achauer U (1995) Imaging a mantle plume beneath the French Massif

1116   Central. Earth and Planetary Science Letters 136:281-296.

1117   Haase KM, Renno AD (2008) Variation of magma generation and mantle sources during

1118   continental rifting observed in Cenozoic lavas from the Eger Rift, Central Europe,

1119   Chemical Geology 257:195-205.

1120   Haase KM, Goldschmidt B, Garbe-Schönberg CD (2004) Petrogenesis of Tertiary continental

1121   intraplate lavas from the Westerwald region, Germany. Journal of Petrology 45:883-

1122   905.

1123   Halliday AN, Lee DC, Tommasini S, Davies GR, Paslick CR, Fitton JG, James DE (1995)

1124   Incompatible trace element in OIB and MORB source enrichment in the sub-oceanic

1125   mantle: Earth and Planetary Science Letters, v. 133, p. 379-395.

1126   Harangi S (2001a) Neogene to Quaternary Volcanism of the Carpathian-Pannonian Region - a

1127   review. Acta Geologica Hungarica. 44:223-258.

1128   Harangi S (2001b) Neogene magmatism in the Alpine-Pannonian Transition zone – a model

1129   for melt generation in a complex geodynamic setting. Acta Vulcanologica, 13:1-11.

1130   Harangi S. (2009): Volcanism of the Carpathian-Pannonian region, Europe: The role of

1131   subduction, extension and mantle plumes. MantlePlumes.org,

1132   http://www.mantleplumes.org/CarpathianPannonian.html, assessed 18 March 2014

1133   Harangi S, Lenkey L (2007) Genesis of the Neogene to Quaternary volcanism in the

1134   Carpathian-Pannonian region: Role of subduction, extension, and mantle plume.

1135   Geological Society of America Special Papers 418:67-92.

1136   Harangi S, Downes H, Thirlwall M, Gméling K (2007) Geochemistry, petrogenesis and

1137   geodynamic relationships of Miocene calc-alkaline volcanic rocks is the Western

1138   Carpathian Arc, eastern central Europe. Journal of Petrology, 48:2261-2287.

1139   Harangi S, Vaselli O, Tonarini S, Szabó C, Harangi R, Coradossi N (1995) Petrogenesis of

1140   Neogene extension-related alkaline volcanic rocks of the Little Hungarian Plain

1141   Volcanic Field (Western Hungary). Acta Vulcanologica, 7:173-187.

1142   Harangi S, Downes H, Seghedi I (2006) Tertiary-Quaternary subduction processes and related

1143   magmatism in the Alpine-Mediterranean region. In: Gee DG, Stephenson RA (eds)

1144   European Lithosphere Dynamics, Geological Society, London, Memoirs, 32:167-190.

1145   Harangi S, Sági T, Seghedi I, Ntaflos T (2013) A combined whole-rock and mineral-scale

1146   investigation to reveal the origin of the basaltic magmas of the Perşani monogenetic

1147   volcanic field, Romania, eastern-central Europe. Lithos 180-181:43-57.

1148   Hart SR (1988) Heterogeneous mantle domains: signatures, genesis and mixing chronologies.

1149   Earth and Planetary Science Letters, 90:273-296.

1150   Herzberg C (2011) Identification of Source Lithology in the Hawaiian and Canary Islands:

1151   Implications for Origins. Journal of Petrology 52:113-146.

1152   Herzberg C, Asimow PD (2008) Petrology of some oceanic island basalts: PRIMELT2.XLS

1153   software for primary magma calculation. Geochemistry Geophysics Geosystem, 9,

1154   Q09001, doi:10.1029/2008GC002057.

1155   Hetényi G, Stuart G, Houseman G, Horvath F. Hegedüs E, Brückl E (2009) Anomalously

1156   deep mantle transition zone below Central Europe: evidence of lithospheric instability,

1157   Geophysical Research Letters, 36:doi: 10.1029/2009GL040171.

1158   Hill R, Roeder P (1974) The Crystallization of Spinel from Basaltic Liquid as a Function of

1159   Oxygen Fugacity. Journal of Geology 82:709-729.

1160 Hirose K, Kawamoto T (1995) Hydrous partial melting of lherzolite at 1 GPa - The effect of

1161 H_2O on the genesis of basaltic magmas. Earth and Planetary Science Letters 133:463-

1162   473.

1163 Hirose K, Kushiro I (1993) Partial melting of dry peridotites at high pressures: determination

1164   of composition of melts segregated from peridotite using aggregate of diamonds. Earth

1165   and Planetary Science Letters, 114:477-489.

1166 Hirschmann MM (2000) Mantle solidus: Experimental constraints and the effects of peridotite

1167   composition, Geochem. Geophys. Geosyst., 1, 1042:doi:10.1029/2000GC000070.

1168 Hirschmann MM (2006) Water, melting, and the deep Earth H_2O cycle. Annual Review of

1169   Earth and Planetary Sciences 34:629-653.

1170 Hirschmann MM, Tenner T, Aubaud C, Withers AC (2009) Dehydration melting of

1171   nominally anhydrous mantle: The primacy of partitioning. Physics of the Earth and

1172   Planetary Interiors 176:54-68.

1173 Hoernle K, Zhang YS, Graham D (1995) Seismic and geochemical evidence for large-scale

1174   mantle upwelling beneath the eastern Atlantic and western and central Europe. Nature

1175   374:34-39.

1176 Horváth F (1993) Towards a mechanical model for the formation of the Pannonian Basin.

1177   Tectonophysics 226:333-357.

1178 Horváth F, Cloetingh S (1996) Stress-induced late-stage subsidence anomalies in the

1179   Pannonian Basin. Tectonophysics 266:287-300.

1180 Horváth F, Faccenna C (2011) Central Mediterranean mantle flow system and the formation

1181   of the Pannonian basin. Geophysical Research Abstracts 13:EGU2011-8894-2.

1182 Horváth F, Dövényi P, Szalay, Á, Royden, L H. 1988. Subsidence, thermal and maturation

1183   history of the Great Hungarian Plain. In: Royden LH, Horváth F (eds) The Pannonian

1184   Basin: a Case Study in Basin Evolution. AAPG Memoirs, 45:355–372.

1185   Horváth F, Bada G, Szafián P, Tari G, Ádám A, Cloetingh S (2006) Formation and

1186   deformation of the Pannonian Basin. In: Gee DG, Stephenson RA (Eds.) European

1187   lithosphere dynamics. Geological Society London Memoirs, 32:191–207.

1188   Huismans RS, Podladchikov YY, Cloething S (2001) Dynamic modeling of the transition

1189   from passive to active rifting, application to the Pannonian basin. Tectonics 20:1021-

1190   1039.

1191   Humphreys ER, Niu Y (2009) On the composition of ocean island basalts (OIB): The effects

1192   of lithospheric thickness variation and mantle metasomatism. Lithos, 112:118-136.

1193   Hurai V, Danišík M, Huraiová M, Paquette JL, Ádám A. (2013) Combined U/Pb and (U-

1194   Th)/He geochronometry of basalt maars in Western Carpathians: implications for age

1195   of intraplate volcanism and origin of zircon metasomatism. Contributions to

1196   Minerology and Petrology, 166:1235-1251.

1197   Jankovics MÉ, Harangi S, Kiss B, Ntaflos T (2012) Open-system evolution of the Füzes-tó

1198   alkaline basaltic magma, western Pannonian Basin: Constraints from mineral textures

1199   and compositions. Lithos, 140-141:25-37.

1200   Jankovics MÉ, Dobosi G, Embey-Isztin A, Kiss B, Sági T, Harangi S, Ntaflos T (2013)

1201   Origin and ascent history of unusually crystal-rich alkaline basaltic magmas from the

1202   western Pannonian Basin. Bulletin of Volcanology, 75:1-23.

1203   Jung C, Jung S, Hoffer E, Berndt J (2006) Petrogenesis of Tertiary mafic alkaline magmas in

1204   the Hocheifel, Germany. Journal of Petrology 47:1637-1671.

1205   Jung S, Pfänder JA, Brügmann G, Stracke A. (2005) Sources of primitive alkaline rocks from

1206   the Central European Volcanic Province (Rhön, Germany) inferred from Hf, Os and

1207   Pb isotopes. Contributions to Mineralogy and Petrology, 150:546-559.

1208   Jung S, Vieten K, Romer RL, Mezger K, Hoernes S, Satir M (2012) Petrogenesis of Tertiary

1209   Alkaline Magmas in the Siebengebirge, Germany. Journal of Petrology 53:2381-2409.

1210   Kamenetsky, V.S, Crawford, A.J, Meffre, S, 2001. Factors controlling chemistry of magmatic

1211   spinel: an empirical study of associated olivine, Cr-spinel and melt inclusions from

1212   primitive rocks. Journal of Petrology 42, 655-671.

1213   Karato S (2011) Water distribution across the mantle transition zone and its implications for

1214   the global material circulation, Earth Planet. Sci. Lett., 301:413-423.

1215   Kawabata H, Hanyu T, Chang Q, Kimura JI., Nichols ARL, Tatsumi Y (2011) The Petrology

1216   and Geochemistry of St. Helena Alkali Basalts: Evaluation of the Oceanic Crust-

1217   recycling Model for HIMU OIB Journal of Petrology 52:791-838

1218   Kereszturi G, Németh K, Csillag G, Balogh K, Kovács J (2011) The role of external

1219   environmental factors in changing eruption styles of monogenetic volcanoes in a

1220   Mio/Pleistocene continental volcanic field in western Hungary. Journal of

1221   Volcanology and Geothermal Research 201:227-240.

1222   Kereszturi G, Németh K, Lexa J, Konecny V, Pécskay Z (2013) Eruptive volume estimate of

1223   the Nógrád-Gömör/Novohrad-Gemer Volcanic Field (Slovakia-Hungary). In Buecher

1224   J., Rapprich V, Tietz O. (Eds.) Abstract Volume & Excursion Guides - Basalt

1225   2013:168 - 169

1226   Klemme S, O'Neill HSC (2000) The near-solidus transition from garnet lherzolite to spinel

1227   lherzolite. Contributions to Mineralogy and Petrology 138:237-248

1228   Klemme S (2004) The influence of Cr on the garnet–spinel transition in the Earth's mantle:

1229   experiments in the system MgO–Cr2O3–SiO2 and thermodynamic modelling. Lithos,

1230   77:639–646.

1231   Kogiso T, Hirschmann MM, Frost DJ (2003) High-pressure partial melting of garnet

1232   pyroxenite: possible mafic lithologies in the source of ocean island basalts. Earth

1233   Planetary Science Letters 216:603-617.

1234   Kogiso T, Hirschmann MM (2006) Partial melting experiments of bimineralic eclogite and

1235   the role of recycled mafic oceanic crust in the genesis of ocean island basalts. Earth

1236   and Planetary Science Letters 249:188-199.

1237   Konečný V, Lexa J, Balogh K, Konečný P (1995) Alkali basalt volcanism in Southern

1238   Slovakia: volcanic forms and time evolution. Acta Volcanologica, 7:167-171.

1239   Konečný V, Lexa J, Balogh K (1999) Neogene-Quaternary alkali basalt volcanism in Central

1240   and Southern Slovakia (Western Carpathians). Geolines 9:67-75.

1241   Konečný V, Kováč M, Lexa J, Šefara J (2002) Neogene evolution of the Carpatho-Pannonian

1242   region: an interplay of subduction and back-arc diapiric uprise in the mantle. EGU

1243   Stephan Mueller Special Publication Series, 1:105-123.

1244   Kostopoulos, D.K, James, S.D. 1992. Parameterization of the melting regime of the shallow

1245   upper mantle and the effects of variable lithospheric stretching on mantle modal

1246   stratification and trace element concentrations in magmas. Journal of Petrology, 33,

1247   665-691.

1248   Kovács I, Falus G, Stuart G, Hidas K, Szabó C, Flower MFJ, Hegedűs E, Posgay K, Zilahi-

1249   Sebess L (2012) Seismic anisotropy and deformation patterns in upper mantle

1250   xenoliths from the central Carpathian-Pannonian region: Asthenospheric flow as a

1251   driving force for Cenozoic extension and extrusion? Tectonophysics, 514-517:168-

1252   179.

1253   Langmuir CH, Forsyth DW (2007) Mantle Melting Beneath Mid-Ocean Ridges.

1254   Oceanography 20:78–89

1255   Langmuir CH, Klein E, Plank T (1992) Petrological systematics of mid-ocean ridge basalts:

1256   Constraints on melt generation beneath ocean ridges. AGU Monograph, 71:183-280.

1257   Le Bas MJ, Le Maitre RW, Streckeisen A, Zanettin B (1986) A chemical classification of

1258   volcanic rocks based on the total alkali silica diagram. - Journal of Petrology, 27:745

1259   750.

1260   Lebedev S, Meier T, van der Hilst RD (2006) Asthenospheric flow and origin of volcanism in

1261   the Baikal Rift area. Earth & Planetary Science Letters, 249:415-424.

1262   Lee CT, Luffi P, Plank T, Dalton H, Leeman WP, (2009) Constraints on the depths and

1263   temperatures of basaltic magma generation on Earth and other terrestrial planets using

1264   new thermobarometers for mafic magmas. Earth and Planetary Science Letters

1265   279:20–33.

1266   Leloup PH, Lacassin R, Tapponnier P, Schärer U, Dalai Z, Xiaohan L, Liangshang Z,

1267   Shaocheng J, Trinh PT (1995) The Ailao Shan–Red River shear zone (Yunnan,

1268   China), Tertiary transform boundary of Indochina. Tectonophysics 251:3-84.

1269   Lenkey L, Dövényi P, Horváth F, Cloetingh S (2002) Geothermics of the Pannonian Basin

1270   and its bearing on the neotectonics. European Geophysical Union Stephan Mueller

1271   Special Publications, Series 3:29-40.

1272   Lexa J, Seghedi I, Németh K, Szakács A, Koneĉny V, Pécskay Z, Fülöp A, Kovacs M (2010)

1273   Neogene-Quaternary volcanic forms in the Carpathian-Pannonian Region: a review.

1274   Central European Journal of Geosciences 2: 207–270.

1275   Lorinczi P, Houseman GA (2010) Lithospheric gravitational instability beneath the Southeast

1276   Carpathians. Tectonophysics, 486:150-150.

1277   Luhr JF, Carmichael ISE (1985) Jorullo volcano, Michoacán, Mexico (1759–1774): The

1278   earlier stages of fractionation in calk-alkaline magmas. Contributions to Mineralogy

1279   and Petrology, 90:142–161

1280   Lustrino M, Wilson M (2007) The Circum-Mediterranean Anorogenic Cenozoic Igneous

1281   Province. Earth-Science Reviews, 81:1–65.

1282   Ma GSK, Malpas J, Xenophontos C, Chan GHN (2011) Petrogenesis of latest

1283   Miocene^Quaternary continental intraplate volcanism along the northern Dead Sea

1284   Fault System (Al Ghab-Homs volcanic field), western Syria: evidence for lithosphere-

1285   asthenosphere interaction. Journal of Petrology 52:401-430.

1286   Martin U, Németh K (2004) Mio/Pliocene Phreatomagmatic Volcanism in the Western

1287   Pannonian Basin: Budapest, Geological Institute of Hungary, 193 p.

1288   Martin M, Wenzel F, CALIXTO Working Group (2006) High-resolution teleseismic body

1289   wave tomography beneath SE Romania: II. Imaging of a slab detachment scenario.

1290   Geophysical Journal International, 164:579–595.

1291   Mayer B, Jung S, Romer RL, Stracke A, Haase KM, Garbe-Schönberg CD. (2013)

1292   Petrogenesis of Tertiary Hornblende-bearing Lavas in the Rhön, Germany. Journal of

1293   Petrology, 54:2095-2123.

1294   Mayer B, Jung S, Romer R, Pfänder JA, Klügel A, Pack A, Gröner E. (2014) Amphibole in

1295   alkaline basalts from intraplate settings: implications for the petrogenesis of alkaline

1296   lavas from the metasomatised lithospheric mantle. Contributions to Mineralogy and

1297   Petrology, 167:DOI: http://doi.org/10.1007/s00410-014-0989-3

1298   McDonough WF, Sun SS (1995) The composition of the Earth. Chemical Geology, 120:223-

1299   253.

1300   McGee LE, Millet MA, Smith IEM, Németh K, Lindsay JM (2012) The inception and

1301   progression of melting in a monogenetic eruption: Motukorea Volcano, the Auckland

1302   Volcanic Field, New Zealand. Lithos 155:360-374.

1303   McGee LE, Smith IEM, Millet MA, Handley HK, Lindsay JM (2013) Asthenospheric Control

1304   of Melting Processes in a Monogenetic Basaltic System: a Case Study of the Auckland

1305   Volcanic Field, New Zealand. Journal of Petrology 54:2125-2153.

1306   McKenzie D (1989) Some remarks on the movement of small melt fractions in the mantle:

1307   Earth Planetary Science Letters, 95:53-72.

1308   Niu Y (2005) Generation and evolution of basaltic magmas: Some basic concepts and a

1309   hypothesis for the origin of the Mesozoic-Cenozoic volcanism in eastern China,

1310   Geological Journal of China Universities, 11:9-46.

1311   Niu Y (2008) The origin of alkaline lavas. Science, 320:883-884.

1312   Niu Y, Wilson M, Humphreys ER, O'Hara MJ (2011) The Origin of Intra-plate Ocean Island

1313   Basalts (OIB): the Lid Effect and its Geodynamic Implications. Journal of Petrology,

1314   52:1443-1468

1315   Ormerod DS, Rogers NW, Hawkesworth CJ (1991) Melting in the lithospheric mantle:

1316   Inverse modelling of alkali-olivine basalts from the Big Pine Volcanic Field,

1317   California. Contributions to Mineralogy and Petrology, 108:305-317.

1318   Panaiotu CG, Jicha BR, Singer BS, Tugui A, Seghedi I, Panaiotu AG, Necula C (2013)

1319   40Ar/39Ar chronology and paleomagnetism of Quaternary basaltic lavas from the

1320   Perşani Mountains (East Carpathians). Physics of the Earth and Planetary Interiors,

1321   221:1-24.

1322   Panaiotu CG, Pécskay Z, Hambach U, Seghedi I, Panaiotu CE, Tetsumaru I, Orleanu M,

1323   Szakács A (2004) Short-lived Quaternary volcanism in the Persani Mountains

1324   (Romania) revealed by combined K-Ar and paleomagnetic data. Geologica

1325   Carpathica, 55:333-339.

1326   Pertermann M, Hirschmann MM (2003) Partial melting experiments on a MORB-like

1327   pyroxenite between 2 and 3 GPa: Constraints on the presence of pyroxenite in basalt

1328   source regions from solidus location and melting rate. Journal of Geophysical

1329   Research: Solid Earth, 108(B2):2125:doi:10.1029/2000JB000118

1330   Pilet S, Hernandez J, Sylvester P, Poujol M (2005) The metasomatic alternative for ocean

1331   island basalt chemical heterogeneity: Earth and Planetary Science Letters, 236:148-

1332   166.

1333   Pilet S, Baker MB, Stolper EM (2008) Metasomatized lithosphere and the origin of alkaline

1334   lavas. Science, 320:916-919.

1335   Piromallo C, Morelli A (2003) P wave tomography of the mantle under the Alpine-

1336   Mediterranean area, Journal of Geophysical Research, 108:doi:

1337   10.1029/2002JB001757

1338   Piromallo C, Vincent AP, Yuen DA, Morelli A (2001) Dynamics of the trasition zone under

1339   Europe inferred from wavelet cross-spectra of seismic tomography. Physics of the

1340   Earth and Planetary Inferiors, 125:125-139.

1341   Popa M, Radulian M, Szakács A, Seghedi I, Zaharia B (2012) New Seismic and Tomography

1342   Data in the Southern Part of the Harghita Mountains (Romania, Southeastern

1343   Carpathians): Connection with Recent Volcanic Activity. Pure Appl. Geophys,

1344   169:1557-1573.

1345   Putirka KD, Kuntz MA, Unruh DM, Vaid N (2009) Magma Evolution and Ascent at the

1346   Craters of the Moon and Neighboring Volcanic Fields, Southern Idaho, USA:

1347   Implications for the Evolution of Polygenetic and Monogenetic Volcanic Fields.

1348   Journal of Petrology, 50:1639-1665.

1349   Robinson JA, Wood BJ (1998) The depth of the spinel to garnet transition at the peridotite

1350   solidus. Earth Planetary of Science Letters, 164:277–284.

1351   Roeder PL, Reynolds I (1991) Crystallization of Chromite and Chromium Solubility in

1352   Basaltic Melts. Journal of Petrology 32:909-934.

1353 Roeder PL, Thornber C, Poustovetov A, Grant A (2003) Morphology and composition of

1354   spinel in Pu'u 'O'o lava (1996-1998), Kilauea volcano, Hawaii. Journal of Volcanology

1355   and Geothermal Research 123:245-265.

1356 Roeder P, Gofton E, Thornber C (2006) Cotectic proportions of olivine and spinel in olivine-

1357   tholeiitic basalt and evaluation of pre-eruptive processes. Journal of Petrology, 47:883-

1358   900.

1359 Royden LH, Horváth F, Burchfiel BC (1982) Transform faulting, extension and subduction in

1360   the Carpathian-Pannonian region: Geological Society of America Bullettin, 93:717-

1361   725.

1362 Rudnick RL, Fountain DM (1995) Nature and composition of the continental crust: a lower

1363   crustal perspective. Reviews of Geophysics, 33:267–309.

1364 Sági T, Harangi S (2013) Origin of the magmas in the Late Miocene to Quaternary Nógrád-

1365   Selmec mongenetic alkali basalt volcanic field, southern-central Slovakia. in : Büchner

1366   J, Rapprich V, Tietz O. (eds) Basalt 2013 Conference Abstract and Excursion Guides,

1367   Görlitz, Germany:17-18.

1368 Sakuyama T, Ozawa K, Sumino H, Nagao K (2009) Progressive melt extraction from

1369   upwelling mantle constrained by the Kita-Matsuura Basalts in NW Kyushu, SW

1370   Japan. Journal of Petrology, 50:725-779.

1371 Salters VJM, Hart SR (1989) The hafnium paradox and the role of garnet in the source of

1372   mid-ocean-ridge basalts. 342:420-422.

1373 Salters VJM, Stracke A (2004) Composition of the depleted mantle. Geochemistry,

1374   Geophysics, Geosystems, 5:Q05B07, doi:10.1029/2003GC000597.

1375 Scarrow JH, Cox KG (1995) Basalts generated by decompressive adiabatic melting of a

1376   mantle plume: a case study from the Isle of Skye, NW Scotland. Journal of Petrology,

1377   36:3-22.

1378 Sclater J, Royden L, Horváth F, Burchfiel B, Semken S, Stegena L. (1980) The formation of

1379   the intra-Carpathian basins as determined from subsidence data. Earth and Planetary

1380   Science Letters, 51:139–162.

1381 Seghedi I, Szakács A (1994) The Upper Pliocene-Pleistocene effusive and explosive basaltic

1382   volcanism from the Perşani Mountains. Rom. J. Petrology 76:101-107.

1383 Seghedi I, Downes H (2011) Geochemistry and tectonic development of Cenozoic

1384   magmatism in the Carpathian–Pannonian region. Gondwana Research 20:655-672.

1385 Seghedi I, Balintoni I, Szakács A (1998) Interplay of tectonics and neogene post-collisional

1386   magmatism in the intracarpathian region. Lithos, 45:483-497.

1387 Seghedi I, Downes H, Szakacs A, Mason PRD, Thirlwall MF, Rosu E, Pecskay Z, Marton E,

1388   Panaiotu C (2004a) Neogene-Quaternary magmatism and geodynamics in the

1389   Carpathian-Pannonian region: a synthesis. Lithos, 72:117-146.

1390 Seghedi I, Downes H, Vaselli O, Szakács A, Balogh K, Pécskay Z (2004b) Post-collisional

1391   Tertiary-Quaternary mafic alkalic magmatism in the Carpathian-Pannonian region: a

1392   review. Tectonophysics 393:43-62.

1393 Seghedi I, Downes H, Harangi S, Mason PRD, Pecskay Z (2005) Geochemical response of

1394   magmas to Neogene-Quaternary continental collision in the Carpathian-Pannonian

1395   region: A review. Tectonophysics, 410:485-499.

1396 Seghedi I, Maţenco L, Downes H, Mason PRD, Szakács A, Pécskay Z (2011) Tectonic

1397   significance of changes in post-subduction Pliocene-Quaternary magmatism in the

1398   south east part of the Carpathian-Pannonian Region. Tectonophysics, 502:146-157.

1399 Shaw DM (1970) Trace element fractionation during anatexis. Geochimica et Cosmochimica

1400   Acta, 34:237-243.

1401 Shaw DM (2000): Continuous (dynamic) melting theory revisited. The Canadian Mineralogist

1402   38:1041-1063

1403 Sigurdsson H, Schilling JG (1976) Spinels in Mid-Atlantic Ridge basalts: Chemistry and

1404   occurrence. Earth and Planetary Science Letters 29:7-20.

1405 Šimon L, Halouzka R (1996) Pútikov vrsok volcano - the youngest volcano in the Western

1406   Carpathians. Slovak Geological Magazine, 2:103-123.

1407 Šimon L, Maglay J (2005) Dating of sediments underlying the Putikov vŕšok volcano lava

1408   flow by the OSL method. Miner. Slovaca 37:279-281.

1409 Smith IEM, Blake S, Wilson CJN, Houghton BF (2008) Deep-seated fractionation during the

1410   rise of a small-volume basalt magma batch: Crater Hill, Auckland, New Zealand.

1411   Contributions to Mineralogy and Petrology, 155:511-527.

1412 Sobolev AV, Shimizu N (1992) Ultradepleted Melts and the Permeability of the Oceanic

1413   Mantle. Dokl. Ross. Akad. Nauk 326:354–360

1414 Sobolev AV, Hofmann AW, Sobolev SV, Nikogosian IK (2005) An olivine-free mantle

1415   source of Hawaiian shield basalts. Nature, 434:590-597.

1416 Sobolev AV, Hofmann AW, Kuzmin DV, Yaxley GM, Arndt NT, Chung SL, Danyushevsky

1417   LV, Elliott T, Frey FA, Garcia MO, Gurenko AA, Kamenetsky VS, Kerr AC,

1418   Krivolutskaya NA, Matvienkov VV, Nikogosian IK, Rocholl A, Sigurdsson IA,

1419   Sushchevskaya NM, Teklay M (2007) The amount of recycled crust in sources of

1420   mantle-derived melts. Science, 316:412-417.

1421 Späth A, Le Roex AP, Opiyo-Akech N. (2001) Plume-Lithosphere Interaction and the Origin

1422   of Continental Rift-related Alkaline Volcanism - the Chyulu Hills Volcanic Province,

1423   Southern Kenya. Journal of Petrology 42:765-787.

1424 Sperner B, Lorenz F, Bonjer K, Hettel S, Muller B, Wenzel F (2001) Slab break-off - abrupt

1425   cut or gradual detachment? New insights from the Vrancea Region (SE Carpathians,

1426   Romania). Terra Nova, 13:172-179.

1427   Sperner B, Ioane D, Lillie RJ (2004) Slab behaviour and its surface expression: new insights

1428   from gravity modelling in the SE-Carpathians. Tectonophysics, 382:51-84.

1429   Stegena L, Géczy B, Horváth F (1975) Late Cenozoic evolution of the Pannonian basin -

1430   Tectonophysics 26:71-90.

1431   Stracke A, Hofmann AW, Hart SR (2005) FOZO, HIMU and the rest of the mantle zoo.

1432   Geochemistry, Geophysics, Geosystems 6:doi:10.1029/2004GC000824.

1433   Strong M, Wolff J (2003) Compositional variations within scoria cones. Geology 31:143-146.

1434   Sun, S, McDonough, W.F, 1989. Chemical and isotopic systematics of oceanic basalts:

1435   implications for mantle compositions and processes. Geological Society Special

1436   Publication, 42, 313-345.

1437   Szabó C, Harangi S, Csontos L (1992) Review of Neogene and Quaternary volcanism of the

1438   Carpathian-Pannonian region. Tectonophysics, 208:243-256.

1439   Szabó C, Falus G, Zajacz Z, Kovács I, Bali E (2004) Composition and evolution of

1440   lithosphere beneath the Carpathian-Pannonian Region: a review. Tectonophysics, 393:

1441   119-137.

1442   Takahashi E, Kushiro I (1983) Melting of a dry peridotite at high pressures and basalt magma

1443   genesis. American Mineralogist, 68:859-879.

1444   Tari G, Dövényi P, Horváth F, Dunkl I, Lenkey L, Stefanescu M, Szafián P, Tóth T (1999).

1445   Lithospheric structure of the Pannonian Basin derived from seismic, gravity and

1446   geothermal data. in: Durand B, Jolivet L, Horváth F, Séranne M. (Eds.) The

1447   Mediterranean Basins: Tertiary extension within the Alpine orogen. Geological

1448   Society, London, Special Publication, 156, pp. 215-250.

1449   Timm C, Hoernle K, van den Bogaard P, Bindeman I, Weaver S (2009) Geochemical

1450   evolution of intraplate volcanism at Banks Peninsula, New Zealand: interaction

1451   between asthenospheric and lithospheric melts. Journal of Petrology 50:989-1023.

1452   Timm C, Hoernle K, Werner R, Hauff F, van den Bogaard P, White J, Mortimer N, Garbe-

1453   Schönberg D (2010) Temporal and geochemical evolution of the Cenozoic intraplate

1454   volcanism of Zealandia. Earth-Science Reviews 98:38-64.

1455   Tschegg C, Ntaflos T, Kiraly F, Harangi S (2010) High temperature corrosion of olivine

1456   phenocrysts in Pliocene basalts from Banat, Romania. Austrian Journal of Earth-

1457   Sciences, 103:101-110.

1458   Valentine GA, Perry FV (2007) Tectonically controlled, time-predictable basaltic volcanism

1459   from a lithospheric mantle source (central Basin and Range Province, USA). Earth and

1460   Planetary Science Letters, 261:201-216.

1461   Vauchez A, Tommasi A, Mainprice, D (2012) Faults (shear zones) in the Earth's mantle.

1462   Tectonophysics, 558-559:1-27.

1463   Wallace M, Green DH (1991) The effect of bulk rock composition on the stability of

1464   amphibole in the upper mantle: Implications for solidus positions and mantle

1465   metasomatism. Mineralogy and Petrology, 44:1-19

1466   Walter MJ (1998) Melting of garnet peridotite and the origin of komatiite and depleted

1467   lithosphere. J. Petrol. 39:29–60.

1468   Wang K, Plank T, Walker JD, Smith EI (2002) A mantle melting profile across the Basin and

1469   Range, SW USA. Journal of Geophysical Research: Solid Earth, 107(B1):ECV 5-1-

1470   ECV 5-21.

1471   Wijbrans J, Németh K, Martin U, Balogh K (2007) 40Ar/39Ar geochronology of Neogene

1472   phreatomagmatic volcanism in the western Pannonian Basin, Hungary. Journal of

1473   Volcanology and Geothermal Research 164:193-204.

1474   Wilson M, Bianchini G (1999) Tertiary-Quaternary magmatism within the Mediterranean and

1475   surrounding regions. in: Durand B, Jolivet L, Horváth F, Séranne M (eds) The

1476   Mediterranean Basins: Tertiary extension within the Alpine orogen, Geological

1477   Society London Special Publication, 156, pp. 141-168.

1478   Wilson M, Downes H (1991) Tertiary-Quaternary extension-related alkaline magmatism in

1479   Western and Central Europe. Journal of Petrology, 32:811-849.

1480   Wilson M, Downes H (2006) Tertiary-Quaternary intra-plate magmatism in Europe and its

1481   relationship to mantle dynamics, In: Stephenson R; Gee D (Ed) European Lithosphere

1482   Dynamics, Geological Society of London Memoir, 32:147-166.

1483   Wilson M, Patterson R. (2001) Intraplate magmatism related to short-wavelength convective

1484   instabilities in the upper mantle: Evidence from the Tertiary-Quaternary volcanic

1485   province of western and central Europe. In: Ernst RE, Buchan KL (Eds) Mantle

1486   Plumes: Their Identification Through Time. Geol. Soc. Amer. Spec. Paper, 352:37-58.

1487   Woodland AB, Jugo PJ (2007) A complex magmatic system beneath the Devés volcanic field,

1488   Massif Central, France: evidence from clinopyroxene megacrysts. Contributions to

1489   Mineralogy and Petrology 153:719-731.

1490   Wortel MJR, Spakman W (2000) Subduction and Slab Detachment in the Mediterranean-

1491   Carpathian Region. Science, 290:1910-1917.

1492   Zou H (1998) Trace element fractionation during modal and nonmodal dynamic melting and

1493   open-system melting; a mathematical treatment. Geochim. Cosmochim. Acta 62:1937-

1494   1945.

1495

Figure captions

1498   Figure 1. – (A) Geological setting and (B) location of the Miocene to Quaternary basalts in

1499   the Carpathian-Pannonian Region with the main tectonic lines (after Horváth et al.,

1500   2006). SVF=Styrian Volcanic Field; BU=Burgenland basalts; KVF=Kemenes

1501   Volcanic Field; BBVF=Bakony-Balaton Upland Volcanic Field; ST= Štiavnica

1502   basalts; KE=Kecel basalts (buried); LU=Lucaret basalt; PVF=Perşani Volcanic Field.

1503   Figure 2. – Classification of the basalts based on the TAS diagram (Le Bas et al. 1986). The

1504   used data set is found in the supplementary table along with the references to the

1505   sources of the data. Data of the Pásztori trachyte is from Harangi et al. (1995) and

1506   Harangi (2001b).

1507   Figure 3. - Selected major elements (in wt%) and trace elements (in ppm) vs. MgO for the

1508   CPR basalts. Symbols as in Fig. 2.

1509   Figure 4. – Primitive mantle (McDonough and Sun, 1995) normalized trace element patterns

1510   for representative CPR basalts. Note that two groups can be distinguished based on the

1511   incompatible trace element abundances and the existence of negative K-anomaly.

1512   Figure 5. – $(La/Yb)_N$ vs. K/K* and $^{143}Nd/^{144}Nd$ vs. K/K* diagrams for the CPR basalts. Note

1513   the negative correlation between these variables suggesting formation of the strongest

1514   negative K-anomaly in the melts generated at small degree of melting where garnet

1515   remained in the residue. The covariance between $^{143}Nd/^{144}Nd$ and K/K* in the

1516   different basalt volcanic fields of the CPR implies that the negative K-anomaly could

1517   be inherited in the mantle source regions. The K/K* is calculated as $K_N/\sqrt{(Nb_N*La_N)}$,

1518   where N denotes normalization to the primitive mantle (McDonough and Sun, 1995)

1519   values. Symbols as in Fig. 2.

1520   Figure 6. – (A) Estimation of the initial and final pressures (p_o and p_f, respectively) of the

1521   melting column for selected CPR basalts using the adiabatic decompression model of

1522   Langmuir et al. (1992). The FeO^t and the Na_2O of the calculated primary magmas of

1523   the CPR basalts yield information on the initial melting pressure and the cessation of

1524   the melting, i.e. the final melting pressure. Each curve represents polybaric mantle

1525   melting lines with different initial melting pressure, i.e. where the ambient mantle

1526   temperature intersects the solidus. Each tick mark represents 0.1 GPa of

1527   decompression. The compositions of the primary magmas at the melting curves

1528   provide the values of the final pressure.

1529   (B) Determination of melting pressure based on the calculated primary magma

1530   compositions of the CPR basalts using the ol'-ne'-qtz' plot of Hirose and Kushiro

1531   (1993). ol'=ol+0.75opx; ne'=ne+0.6ab; qtz'=qtz+0.4ab+0.25opx, where ol, opx, ne,

1532   ab, qtz are CIPW normative mineral components. Melting pressure lines are after

1533   Sakuyama et al. (2009).

1534   Figure 7. – Calculated melting columns for different basalts (based on Langmuir et al., 1992

1535   model) compared with the present lithosphere-asthenpshere boundary (LAB) beneath

1536   the volcanic fields that is inferred from interpretation of seismic data (Horváth et al.,

1537   2006). Mantle potential temperatures are given using the calculation scheme of Lee et

1538   al. (2009) using molar Fe^{3+}/Fe^{tot}=0.13. Beneath the Perşani volcanic field Dérerova et

1539   al. (2006) and Horváth et al. (2006) suggested a thick lithosphere (about 140 km),

1540   whereas Martin et al. (2006) indicated much thinner lithosphere. Our melting column

1541   calculation for the Perşani basalts is consistent with the proposed lithosphere thickness

1542   of Martin et al. (2006).

1543   Figure 8. – Comparison of the melting pressure obtained by the calculation procedure of Lee

1544   et al. (2009) with the final melting pressure (p_f) provided by the Langmuir et al. (1992)

1545 model. There is a reasonably good correlation between these pressure values. Symbols

1546 as in Fig. 2.

1547 Figure 9. - Trace element modelling for the melt generation of the CPR basaltic magmas.

1548 Model parameters: critical melting model (critical melt fraction is 0.01) proposed by

1549 Sobolev and Shimizu (1992) with the following source rocks: spinel-lherzolite –

1550 olivine (57%), orthopyroxene (25.5%), clinopyroxene (15%), spinel (2.5%); garnet-

1551 lherzolite - olivine (60.1%), orthopyroxene (18.9%), clinopyroxene (13.7%), garnet

1552 (7.3%). Melting modes are ol1.21opx8.06cpx76.37sp14.36 for sp-lherzolite and

1553 ol1.3opx8.7cpx36gt54 for garnet-lherzolite, respectively. Source rock composition: La

1554 and Nb - 4 x primitive mantle values (2.59 and 2.63 ppm, respectively), Zr - 2 x

1555 primitive mantle values (21 ppm) and Y – 1.5 x primitive mantle values (6.45 ppm,

1556 where primitive mantle values are from McDonough and Sun, 1995). Distribution

1557 coefficients are from Kostopoulos and James (1992). Tick marks indicate the degree

1558 of melting at each melting model. Symbols are explained in Fig. 2.

1559 Figure 10. – Melting conditions beneath the Carpathian-Pannonian region in a pressure-

1560 temperature diagram. The position of the melting columns is based on the result of the

1561 Langmuir et al. (1992) model combined with the mantle potential temperature and

1562 melting pressure values calculated by the thermbarometer of Lee et al. (2009). The

1563 melting columns of the basaltic magmas are just below the dry peridotite solidus (as

1564 defined by Hirschmann, 2000). This requires either some water or a more fusible

1565 material, such as pyroxenite or eclogite in the mantle source. Hydrous peridotite solidi:

1566 Hirschmann (2006); pyroxenite (MIX1G) pyroxenite solidus: Kogiso et al. (2003);

1567 MORB-like pyroxenite solidus: Pertermann and Hirschmann (2003). UMX: position

1568 of the ultramafic peridotite xenoliths as given by Embey-Isztin et al. (2001) and

1569 Kovács et al. (2012).

1570 Figure 11. - Compositional characteristics of spinel inclusions in olivine phenocrysts of the

1571   CPR basalts based on the Cr-Fe^{3+}-Al diagram. The most primitive spinels form four

1572   compositionally coherent groups that can be related to the existence of different

1573   mantle domains in the source regions of the basaltic magmas. Note that three of these

1574   groups are present beneath each volcanic fields of the CPR. MORB and OIB spinel

1575   fields are as defined by Barnes and Roeder (2001). Compositional data of spinels are

1576   from Jankovics et al. (2012), Harangi et al. (2013) and Sági et al. (in prep).

1577 Figure 12. – Position of the basalt volcanic fields in the CPR compared with the seismically

1578   defined lithosphere-asthenosphere boundary lines (Horváth et al., 2006). Note that the

1579   volcanic fields are located at the margin of the Pannonian basin and not in the central

1580   parts where the lithosphere is the thinnest.

1581 Figure 13. – Conceptual model for the triggering of melt generation beneath the Pannonian

1582   basin. See text for explanation.

1583

1584 Table 1 – Representative major and trace element composition of the basalts from different

1585   volcanic fields of the CPR. Reference: 1: Ali et al. (2013), 2: Ali and Ntaflos (2011),

1586   3: this study, 4: Harangi et al. (2013). p_f and p_o are the calculated final and initial

1587   melting pressures using the Langmuir et al. (1992) model. T and p are the mantle

1588   potential temperature and the melting pressure using the thermobarometer of Lee et al.

1589   (2009) with molar Fe^{3+}/Fe^{tot}=0.13.

Figure 1A
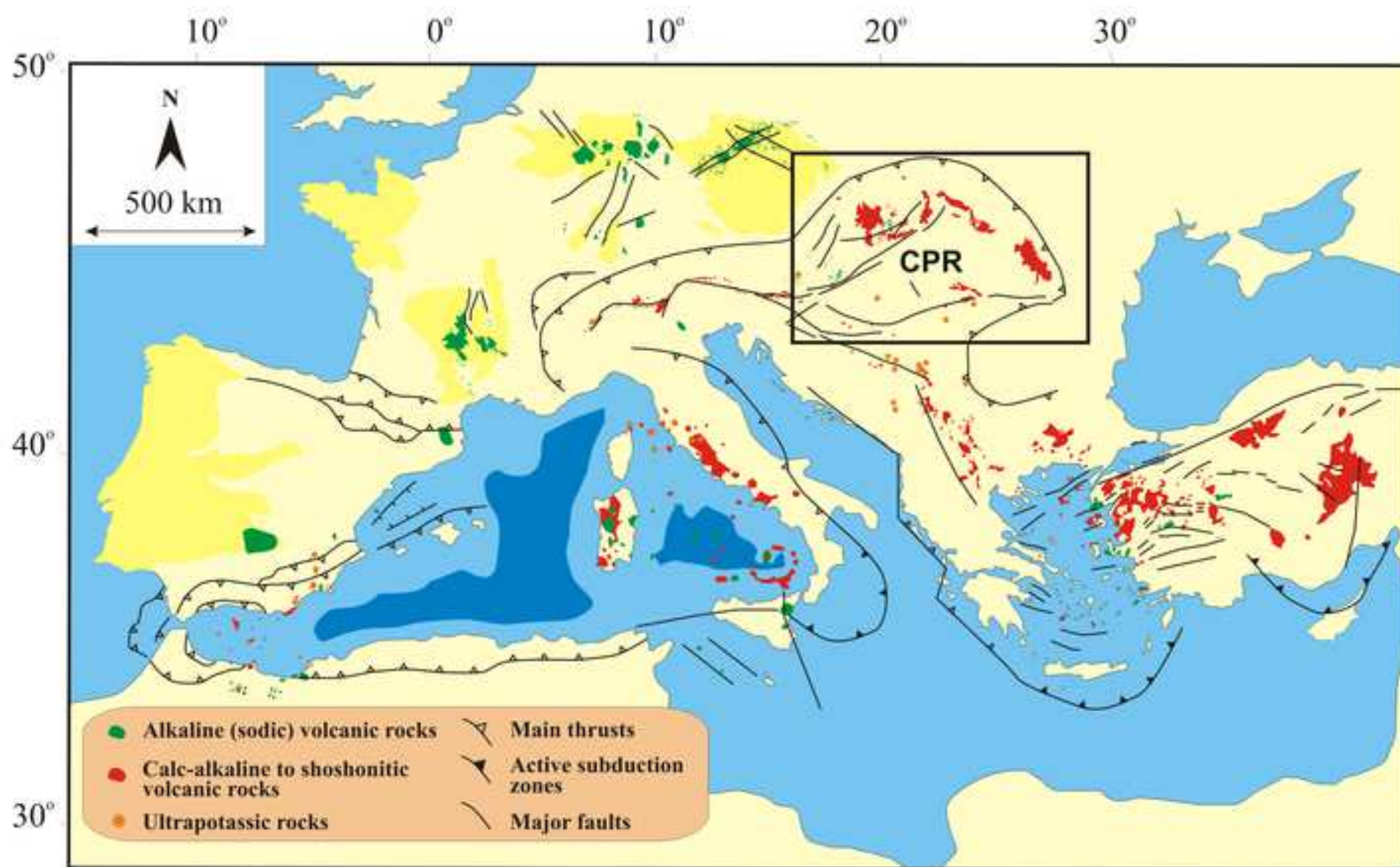
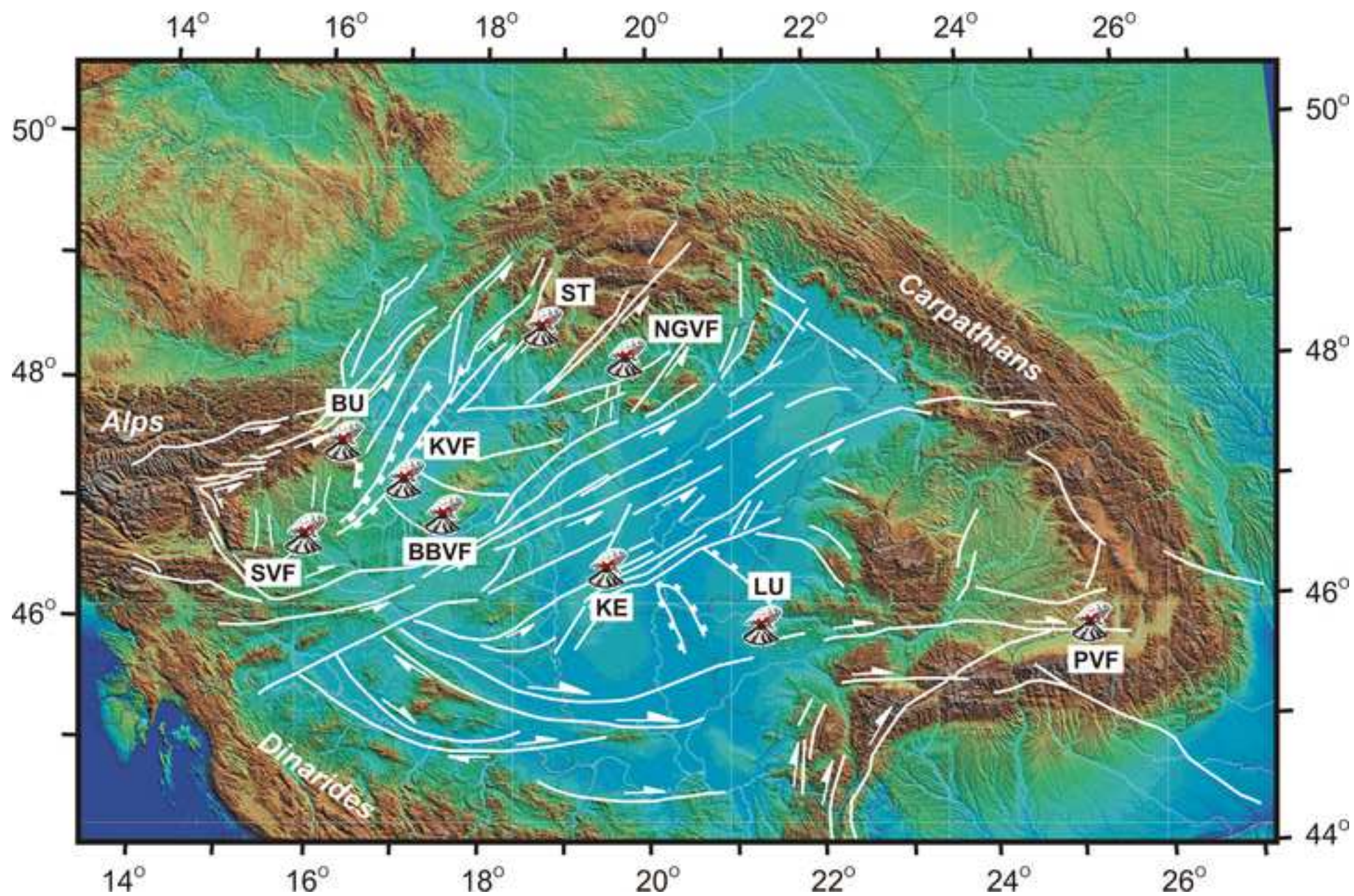Figure 2
Click here to download high resolution image
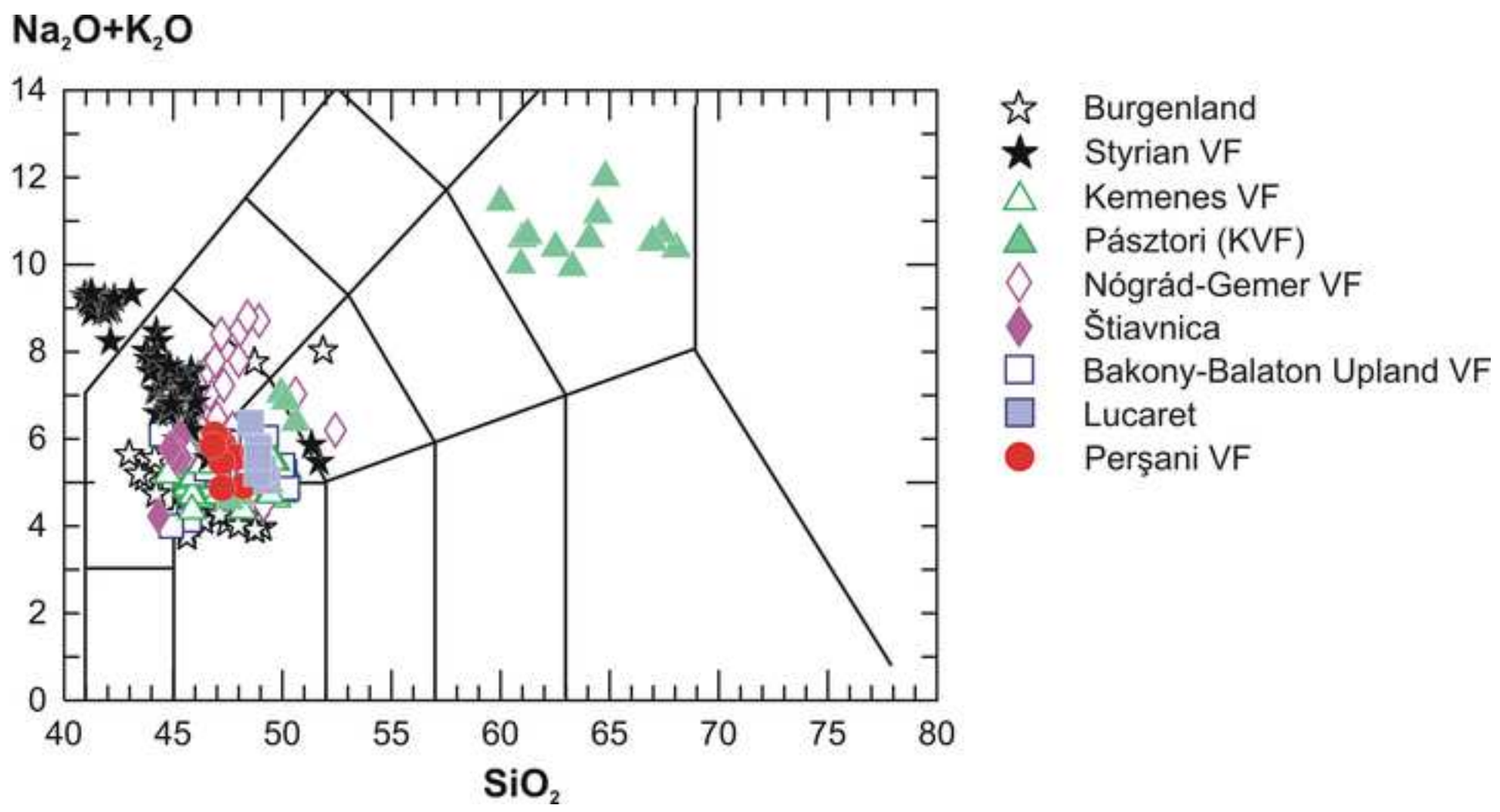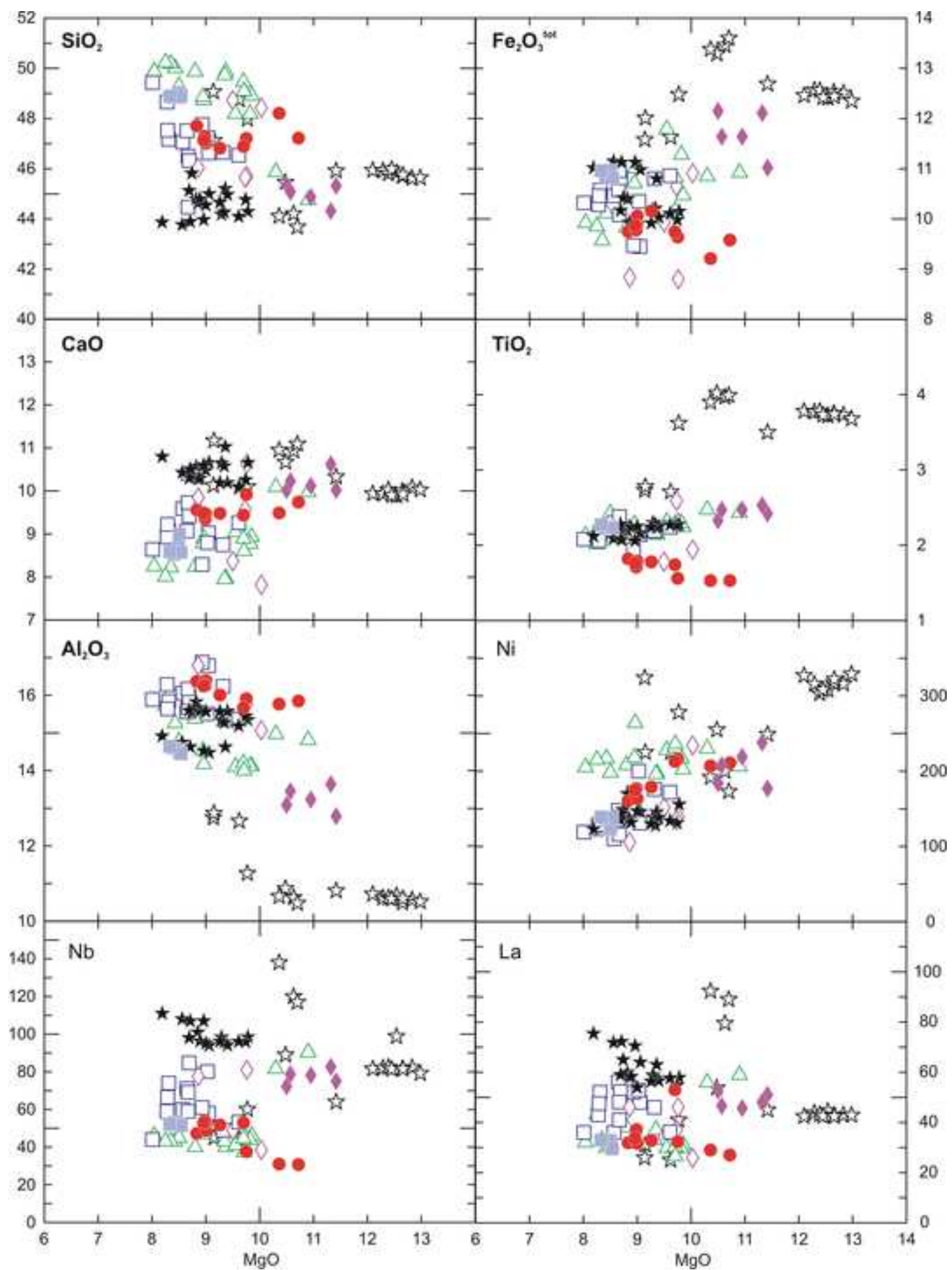
Figure 3
Click here to download high resolution image

Figure 4
Click here to download high resolution image

Figure 5
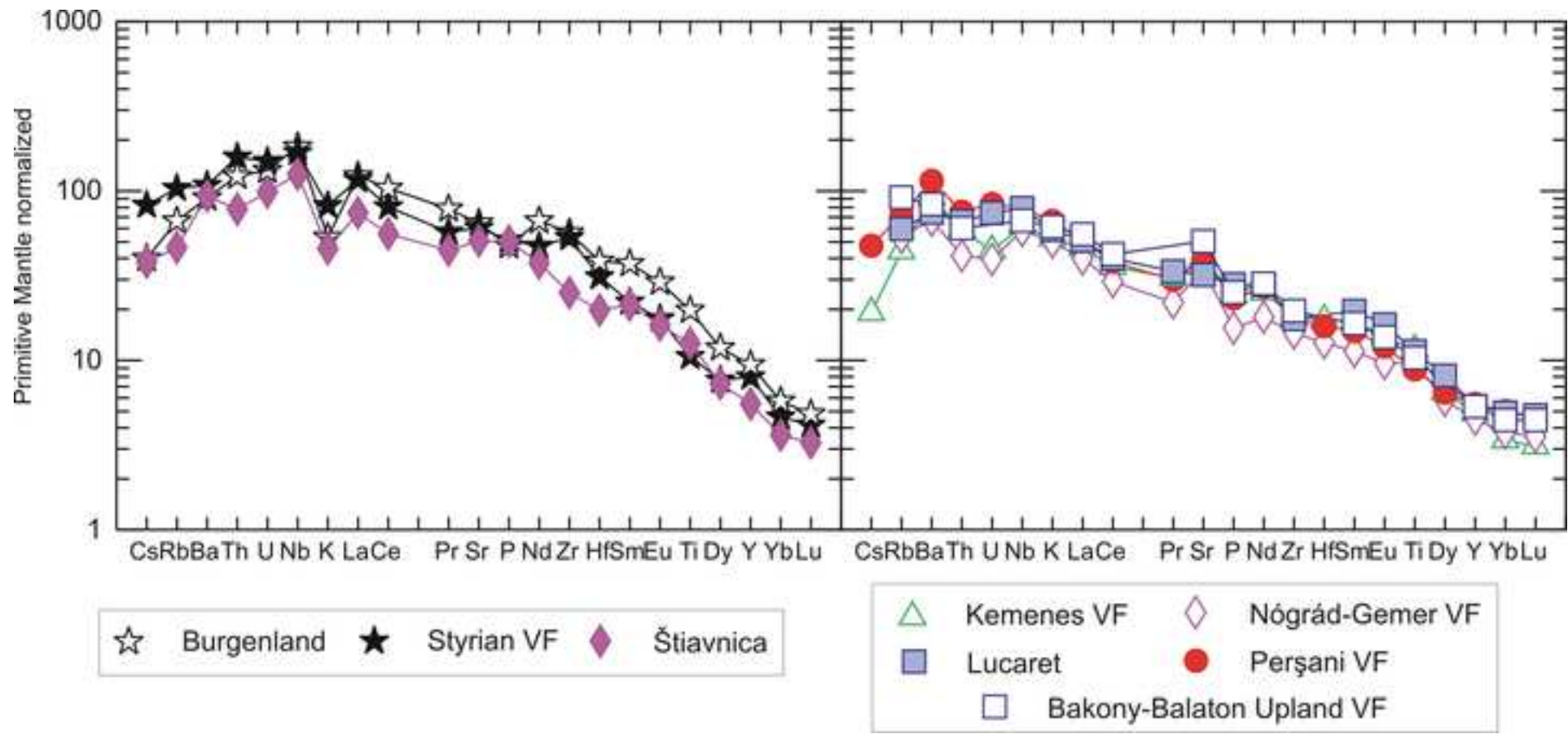Click here to download high resolution image

Figure 6A

Figure 7
Click here to download high resolution image

Figure 8
Click here to download high resolution image
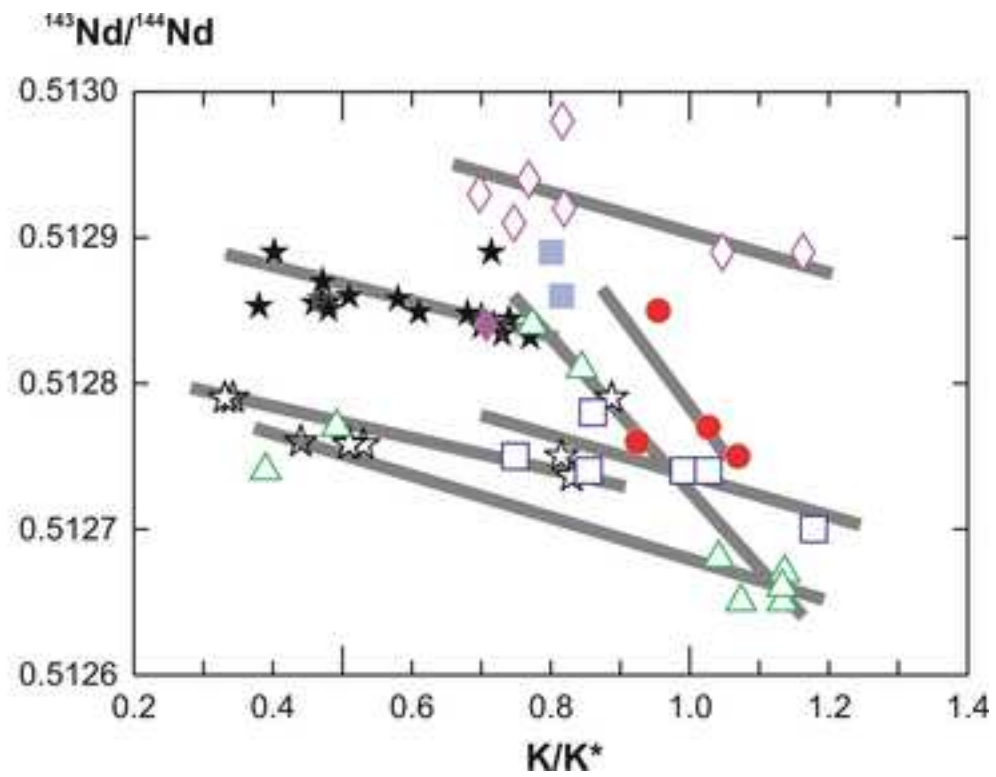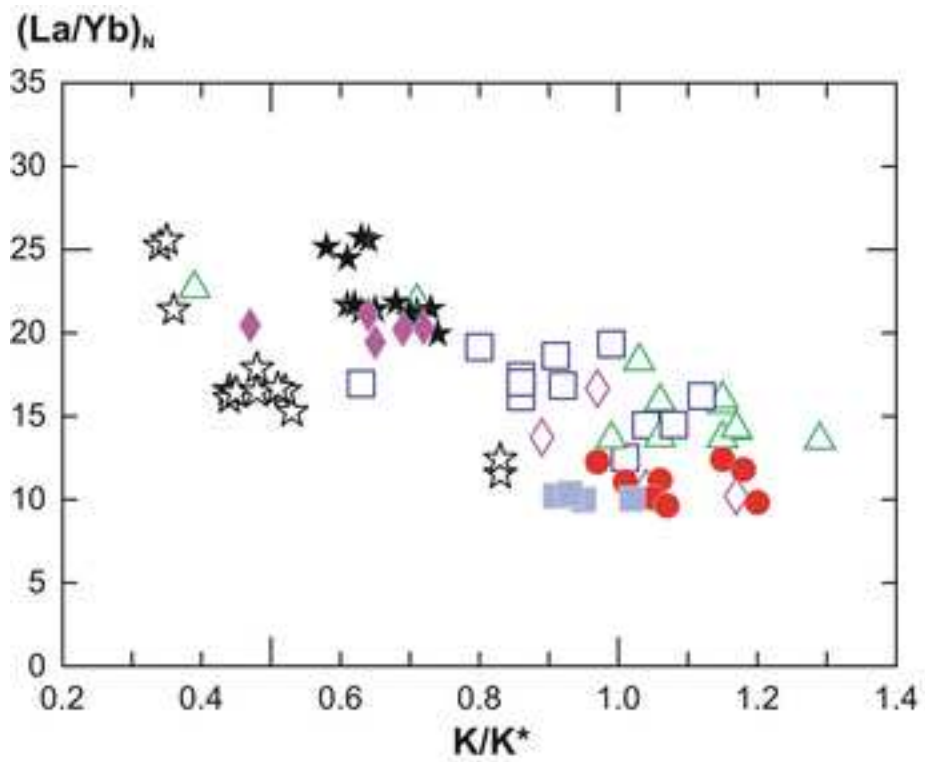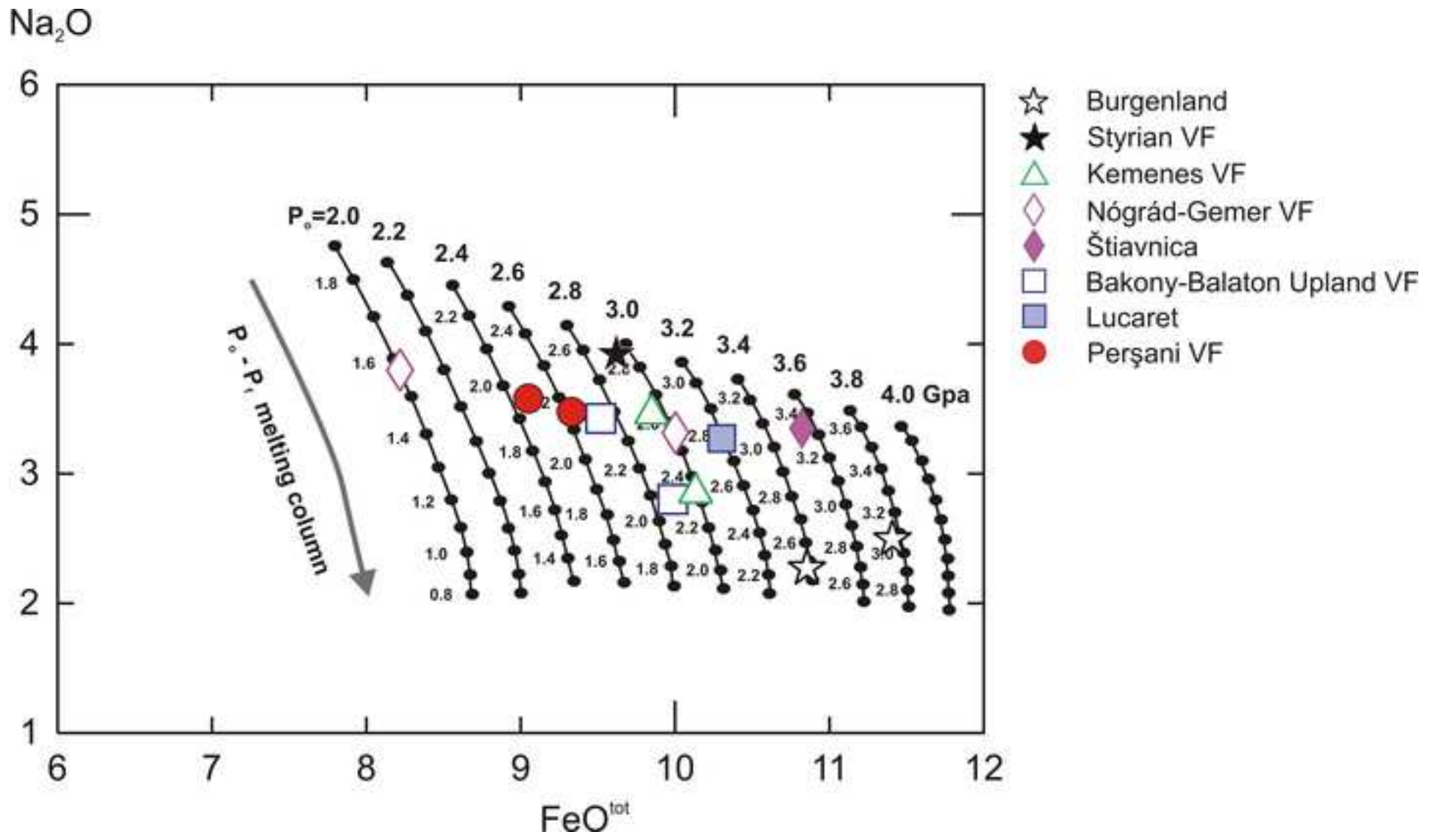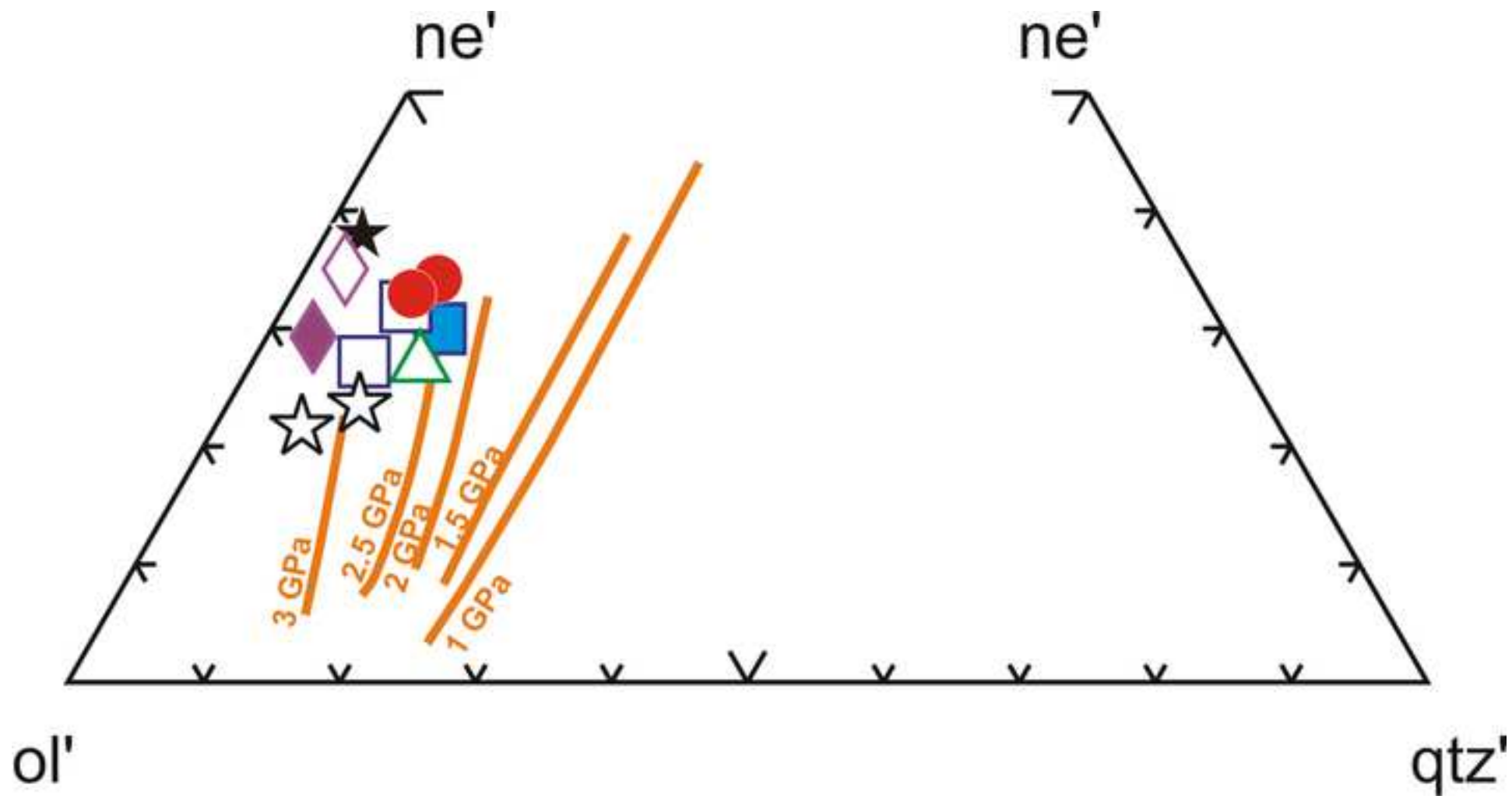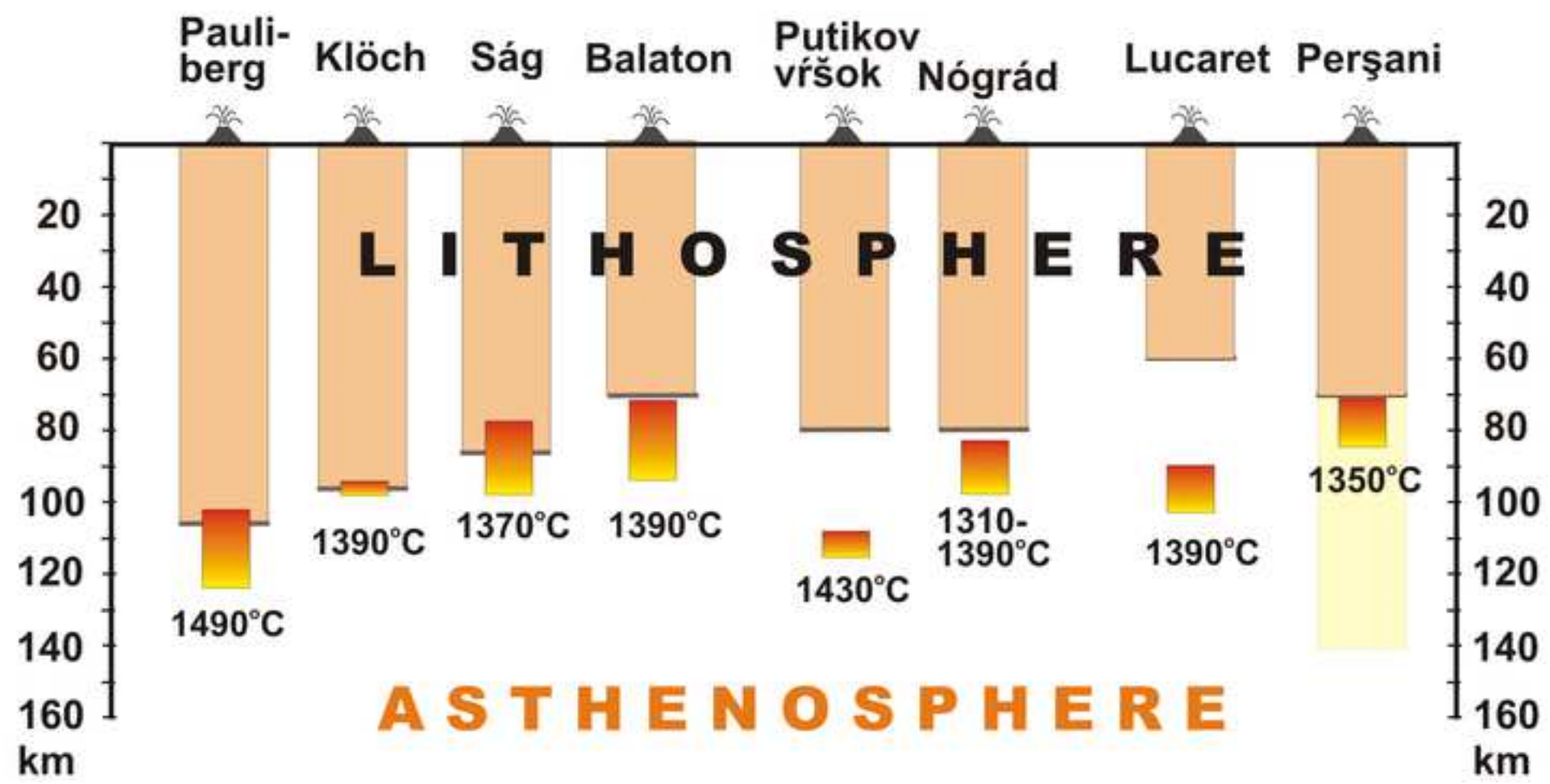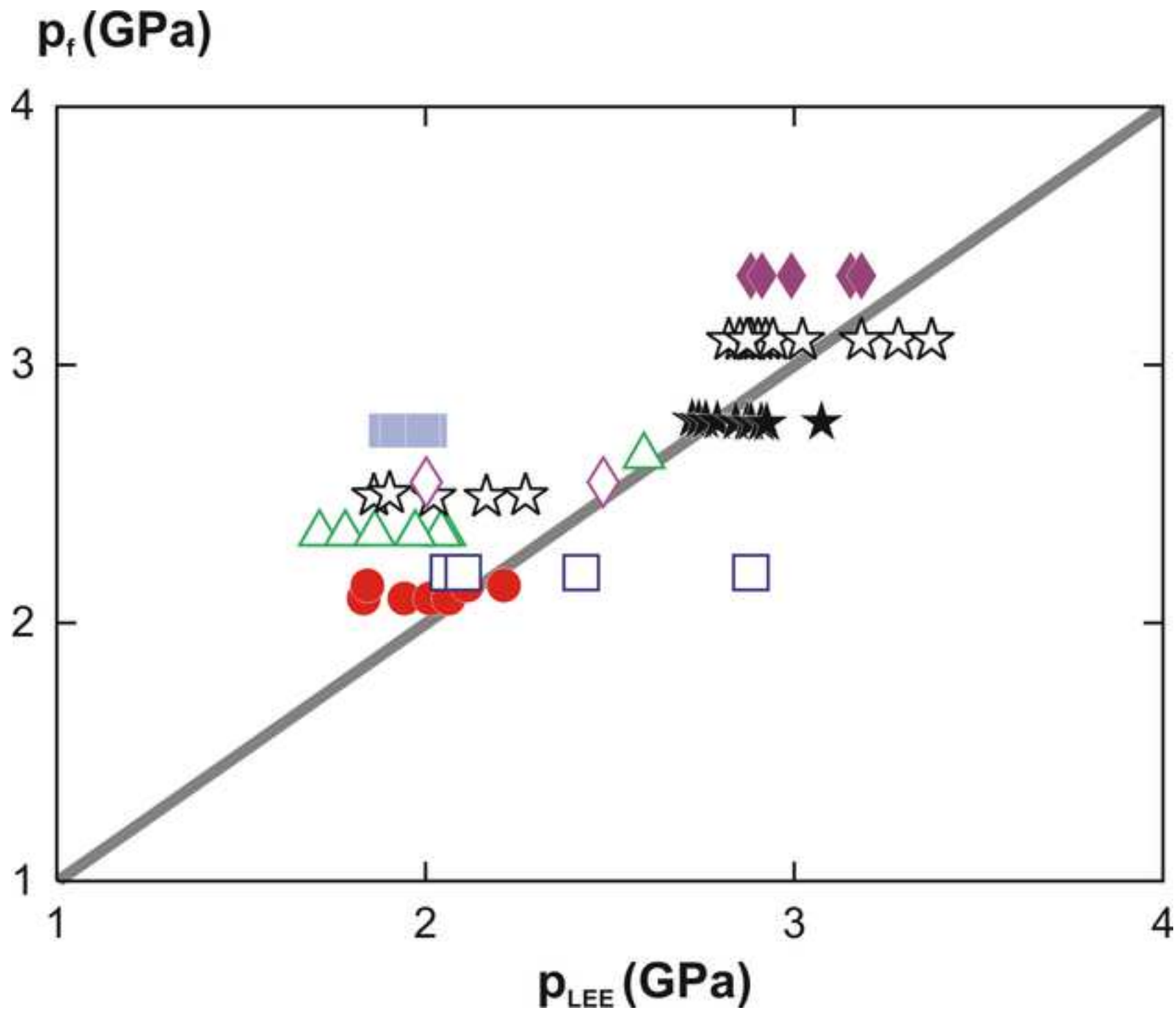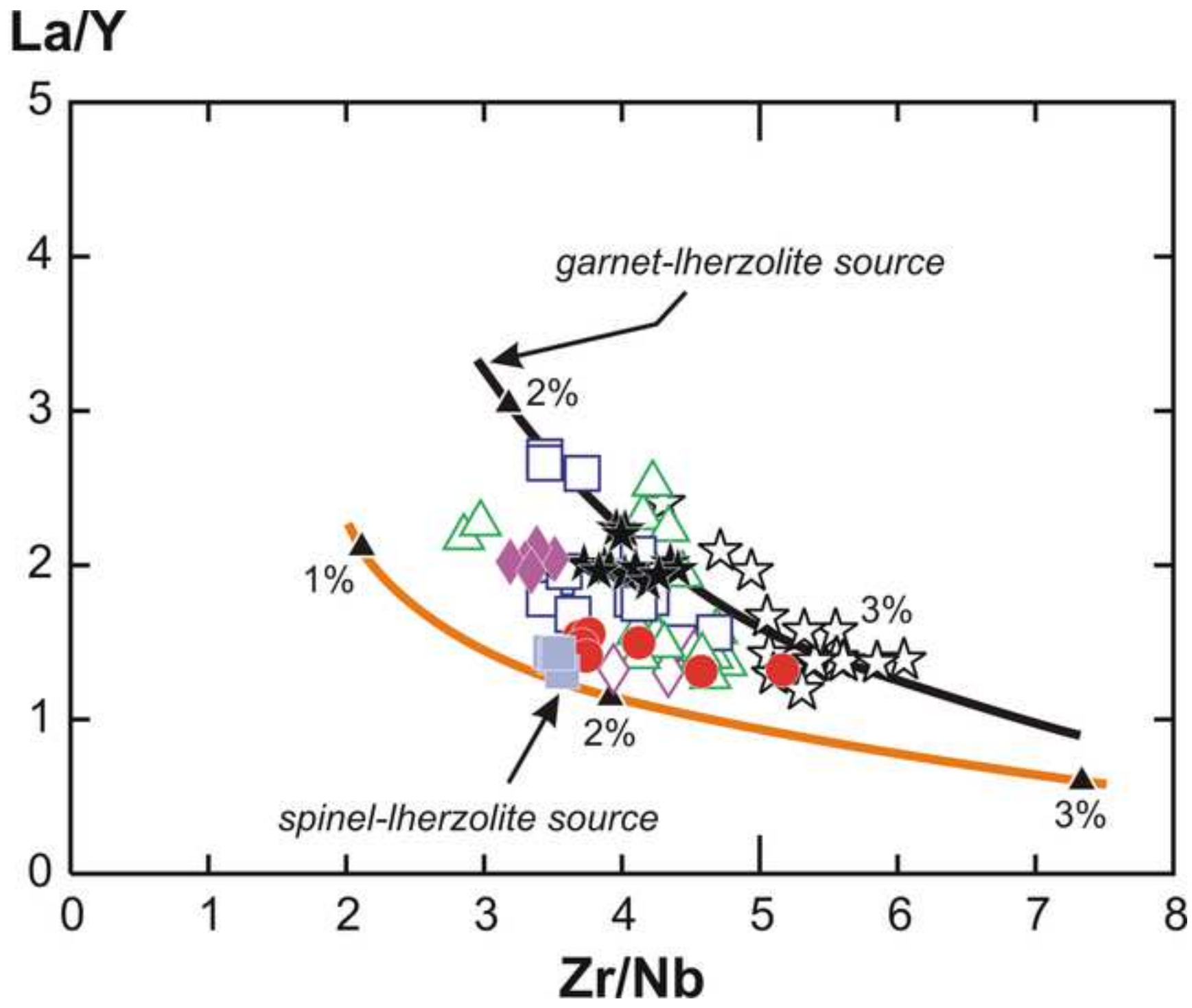
Figure 9
Click here to download high resolution image
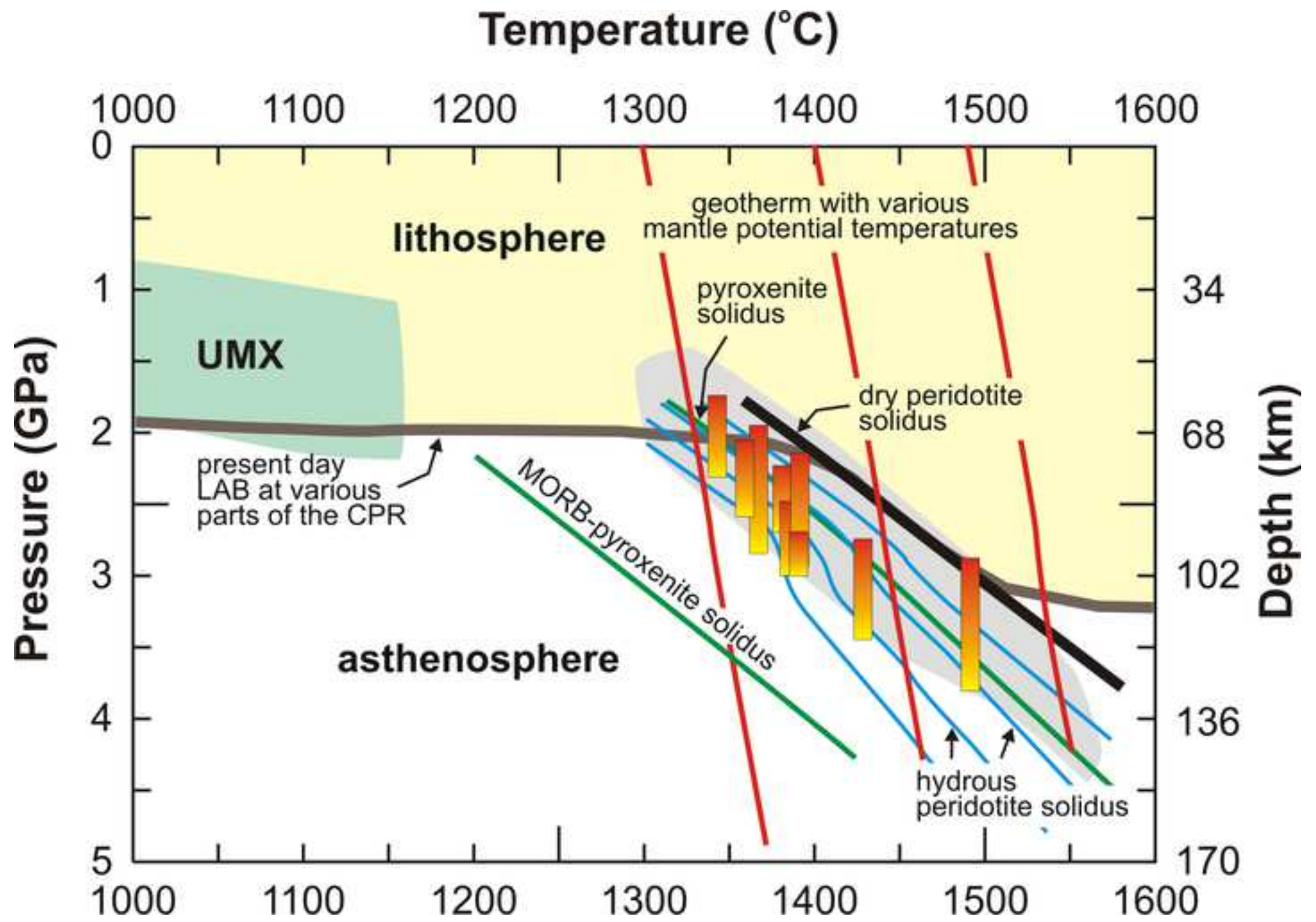
Figure 10
Click here to download high resolution image

Figure 10

Figure 11
Click here to download high resolution image

Figure 12
Click here to download high resolution image

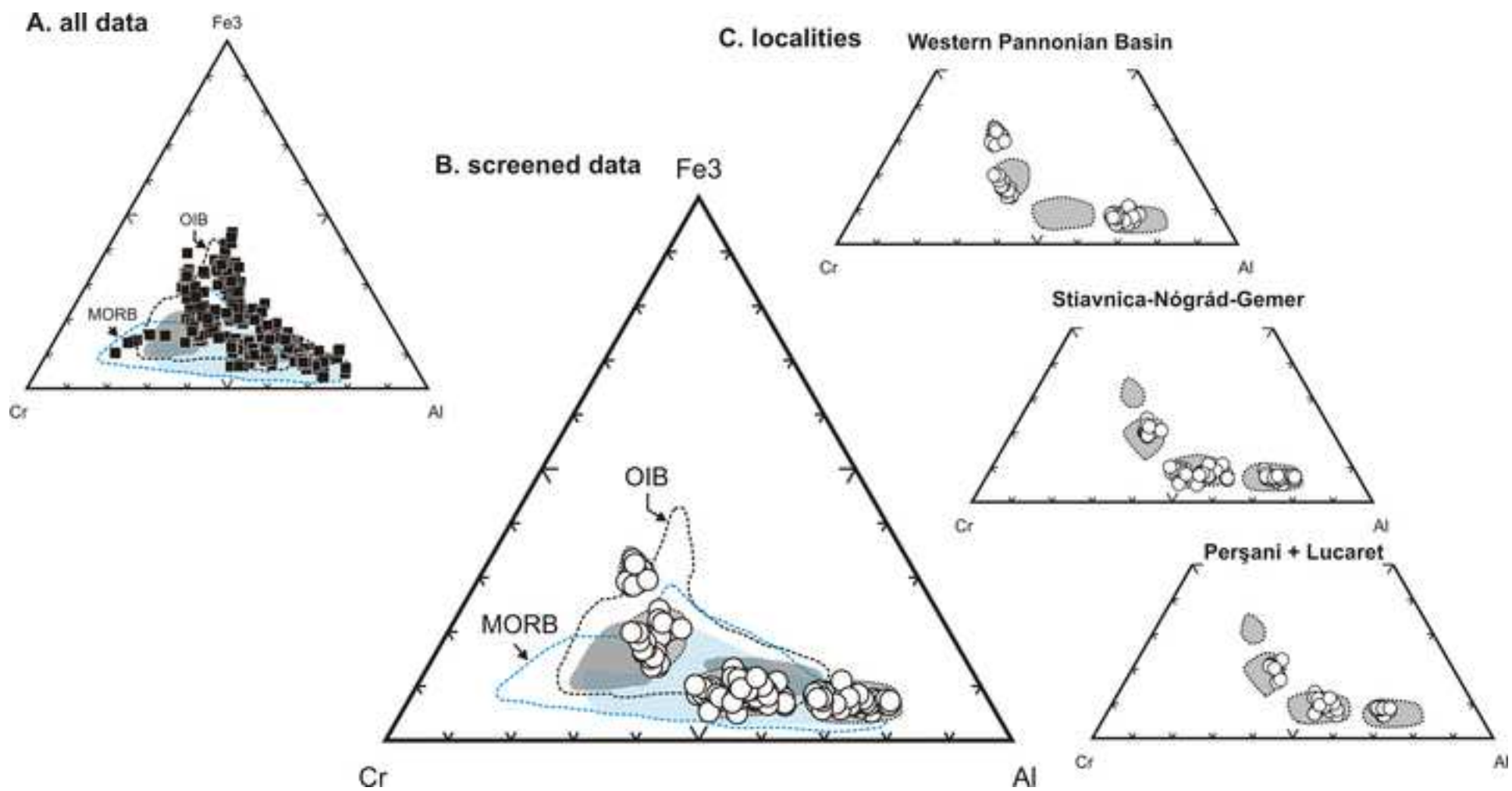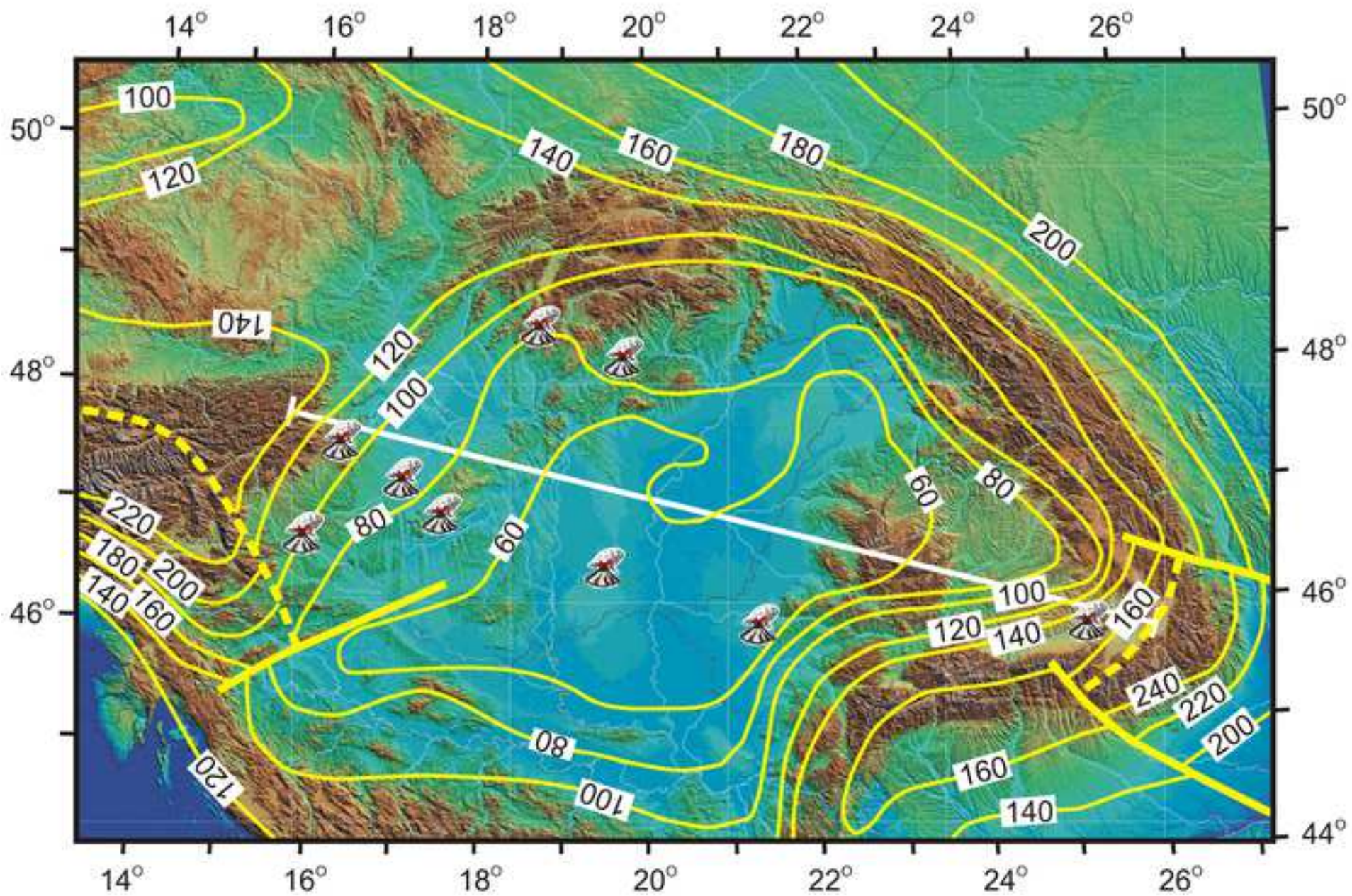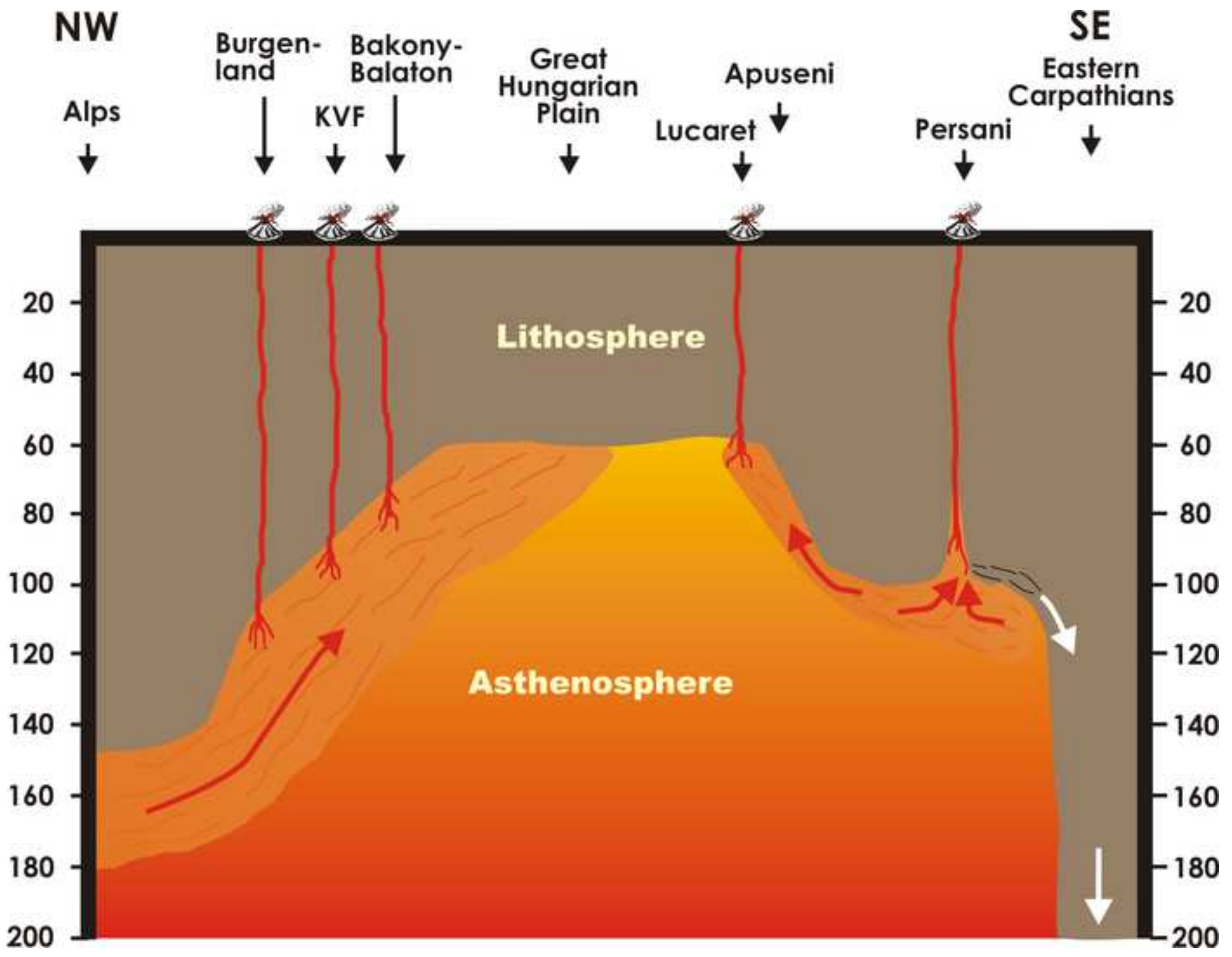Figure 13

Table 1

sample	KL-4	ST-11	PLB-4	OB-1	SAG08-2	S-1	KK-1
locality	Klöch	Steinberg	Pauliberg	Oberpul-lendorf	Ság	Sátorma	Kapolcs
volcanic field	SVF	SVF	BU	BU	KVF	BBVF	BBVF
Reference	1	1	2	2	3	3	3
SiO2	44.97	43.87	46.99	49.07	48.19	47.24	46.53
TiO2	2.25	2.12	3.76	2.73	2.31	2.18	2.24
Al2O3	15.58	14.92	11.13	12.75	14.10	15.51	15.37
Fe2O3t	10.03	11.02	12.59	11.58	11.79	10.35	10.86
MnO	0.17	0.20	0.15	0.20	0.14	0.16	0.15
MgO	9.40	8.19	10.54	9.14	9.55	9.03	9.61
CaO	10.19	10.80	9.95	10.13	9.04	8.80	9.26
Na2O	4.58	5.47	2.78	2.65	2.83	3.65	3.13
K2O	2.11	2.37	1.48	1.31	1.53	2.30	2.18
P2O5	0.72	1.06	0.62	0.44	0.50	0.79	0.67
LOI	0.98	0.23	0.11	2.12	2.1	1.6	1.4
mg-number	0.69	0.63	0.66	0.65	0.65	0.67	0.67
S.I.	-27.25	-38.32	-3.19	2.40	-0.44	-12.19	-10.31
Ni	138	123	274	324	228	200	172
Cr	136	121	332	287	356	246	260
V	215	206	172	200	198	182	176
Sc	19.4	13.6	16.4	20.9	21	19	22
Co	38.1	36	51.5	45.6	48.7	41.4	41.4
Rb	52.8	62.2	39.8	21.2	26.5	56.8	50.7
Ba	581	713	479	305	602	877	627
Sr	1008	1203	881	577	808.1	1159.2	1385.8
Zr	368	556	498	364	187.8	282.9	194.7
Nb	94.2	111	72.4	49.8	40.9	80.1	53.3
Y	28.5	34.3	31.4	27.3	21.1	27.5	21.5
Th	9.9	12.6	5.26	3.64	4.7	8.8	6.7
La	56.6	75.4	43.4	25.9	29.8	52.9	36.2
Ce	104	135	94.8	64.2	59.8	101.3	72.1
Pr	11.4	14.5	12.1	6.9	7.81	12.2	9.11
Nd	46.2	59	49.7	30.7	31.6	48.7	37.8
Sm	7.26	8.97	10.5	6.16	6.87	8.13	6.69
Eu	2.24	2.71	3.07	1.92	2.13	2.36	2.05
Gd	6.68	8.09	9.2	5.82	5.86	6.76	5.67
Tb	0.87	1.02	1.23	0.806	0.85	0.8	0.73
Dy	4.45	5.15	5.89	4.11	4.37	4.86	4.22
Ho	0.82	0.94	1.04	0.755	0.74	0.84	0.78
Er	2.1	2.43	2.53	1.87	1.87	2.21	1.95
Tm	0.28	0.32	0.312	0.249	0.28	0.31	0.28
Yb	1.8	2.04	1.91	1.53	1.49	1.88	1.52
Lu	0.25	0.28	0.246	0.21	0.21	0.28	0.24
Hf	5.96	8.82	9.32	6.16	4.9	6	4.8
Ta	5.12	6.82	3.43	2.69	2.1	4.5	3.3
U	2.54	3.03	1.57	0.917	0.9	2.3	1.8
p_f	2.8		3.1	2.5	2.35	2.2	2.2
p_o	2.9		3.8	3.8	3	2.8	2.9
T	1390		1472	1416	1376	1343	

p   2.72   2.61   1.86   2.05   2.10

PUT-2 Putikov	CSAM1 Belinsky vrch	LU52 Lucaret	BARC Barc
SE	NGVF	LU	PVF
3	3	3	4
44.32	48.43	48.90	46.82
2.53	1.94	2.23	1.78
13.64	15.07	14.45	16.01
12.11	10.91	10.82	10.16
0.19	0.16	0.15	0.17
11.32	10.03	8.54	9.26
10.62	7.82	8.58	9.48
2.91	3.86	4.00	3.93
1.32	1.45	1.76	1.92
1.04	0.32	0.57	0.48
2.4	0.2	-0.4	-0.1
0.69	0.68	0.65	0.68
-11.85	-6.60	-8.17	-16.11
238	234	138	179
383	191.5766	177	315
216	180	144	194
24	19	10.1	26
47.8	51.2	41.4	41.1
27.8	32	36	43.1
617	445	464	758
1011	684.5	627	775
262.9	152	183	185.3
82.6	38.5	51.4	51.8
23.8	19.4	22.6	23.8
6.2	3.3	4.72	6
48.1	25.8	29.5	32.8
93.4	48.9	60	63.9
11.35	5.57	7.61	7.59
46.9	22.5	31.5	34
8.65	4.6	7.12	6.04
2.49	1.48	2.23	1.86
6.86	4.42	6.28	5.14
0.83	0.71	0.94	0.7
4.91	3.92	4.92	4.35
0.8	0.7	0.94	0.83
1.99	1.91	2.38	2.26
0.27	0.27	0.31	0.34
1.6	1.65	2	2.21
0.22	0.24	0.28	0.31
5.6	3.6		4.5
4.8	2.4	2.85	3.1
2	0.8	1.35	1.7
3.35	2.55	2.75	2.15
3.6	3	3.2	2.6
1418	1386	1395	1378

2.91   2.00   1.99   2.21

Electronic Supplementary Material

Click here to download Electronic Supplementary Material: Supplementary_data.xlsx